Figure 1

Click here to access/download;Figure;Figure1.tif

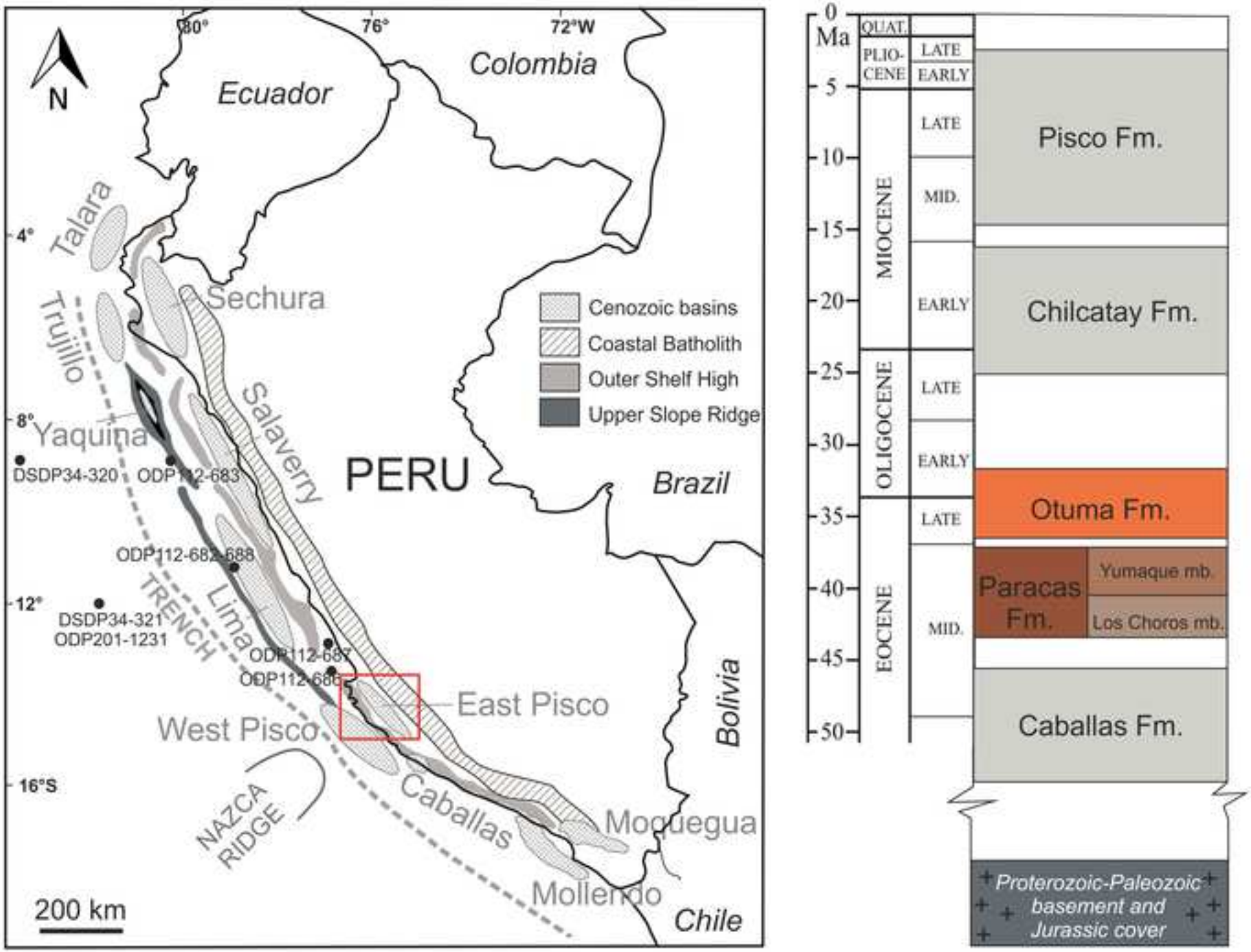

Figure 2

Click here to access/download;Figure;Figure2-ultimiss.JPG

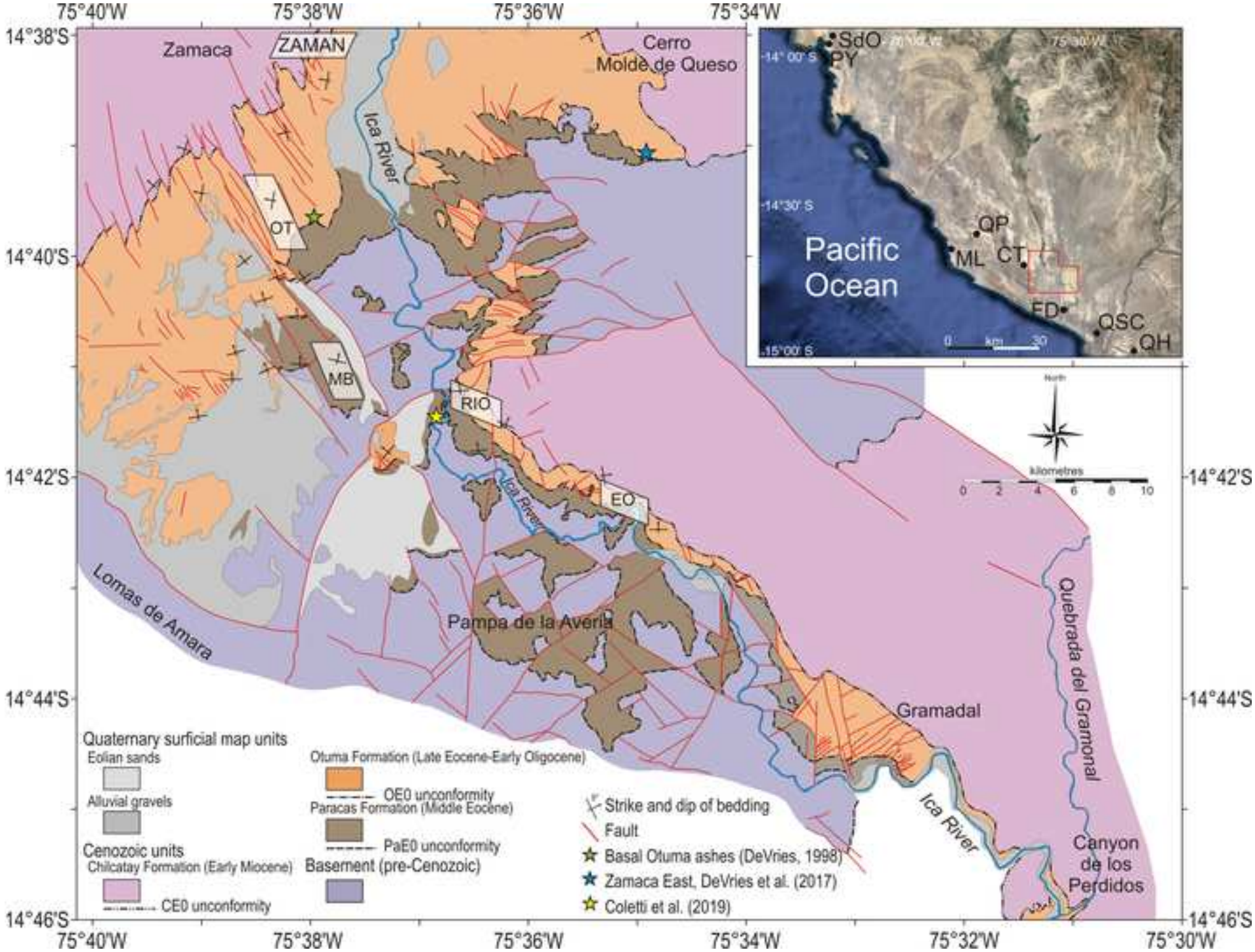

Figure 3

Click here to access/download;Figure;Figure3_reviewedjuly2021.tif

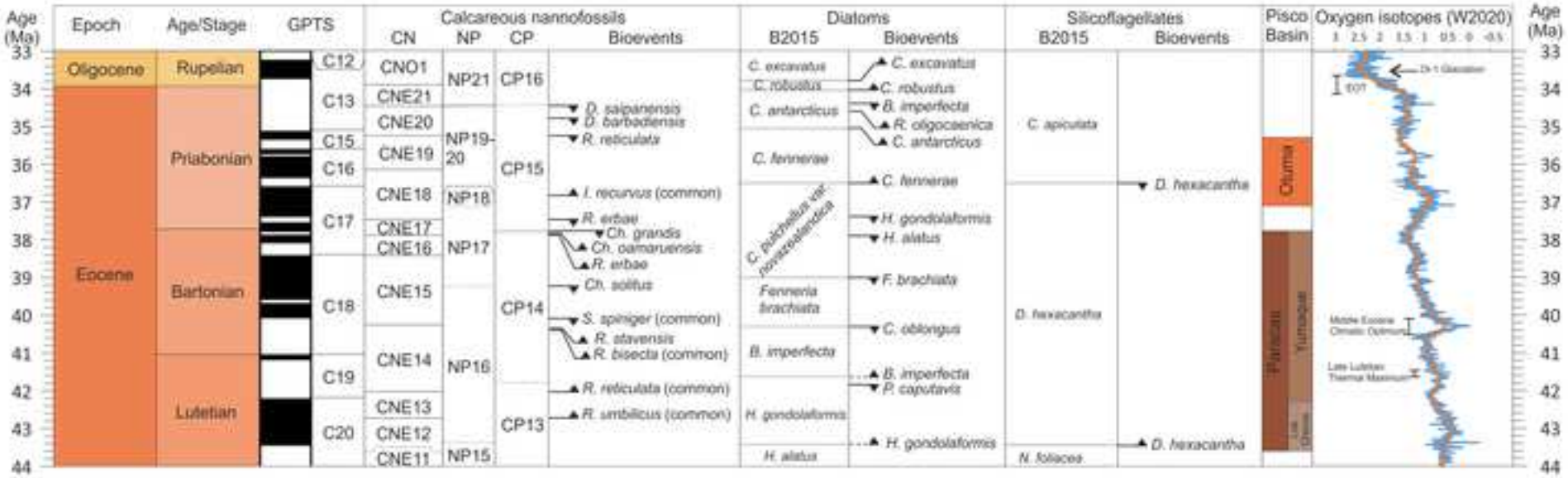

Figure 4-part1

Click here to access/download;Figure;Figure4ad.jpg

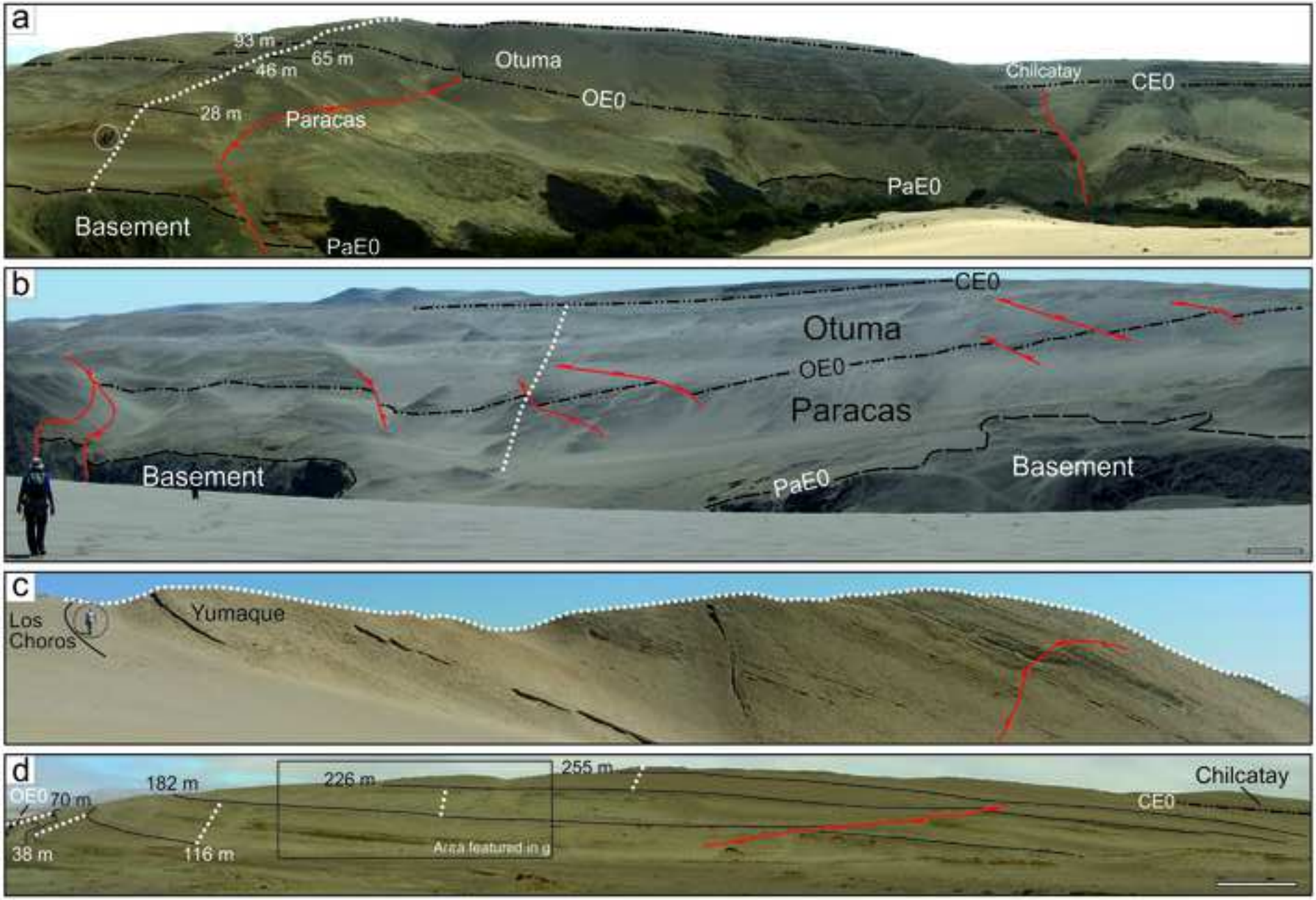

Figure 4-part2

Click here to access/download;Figure;Figure4ei.jpg

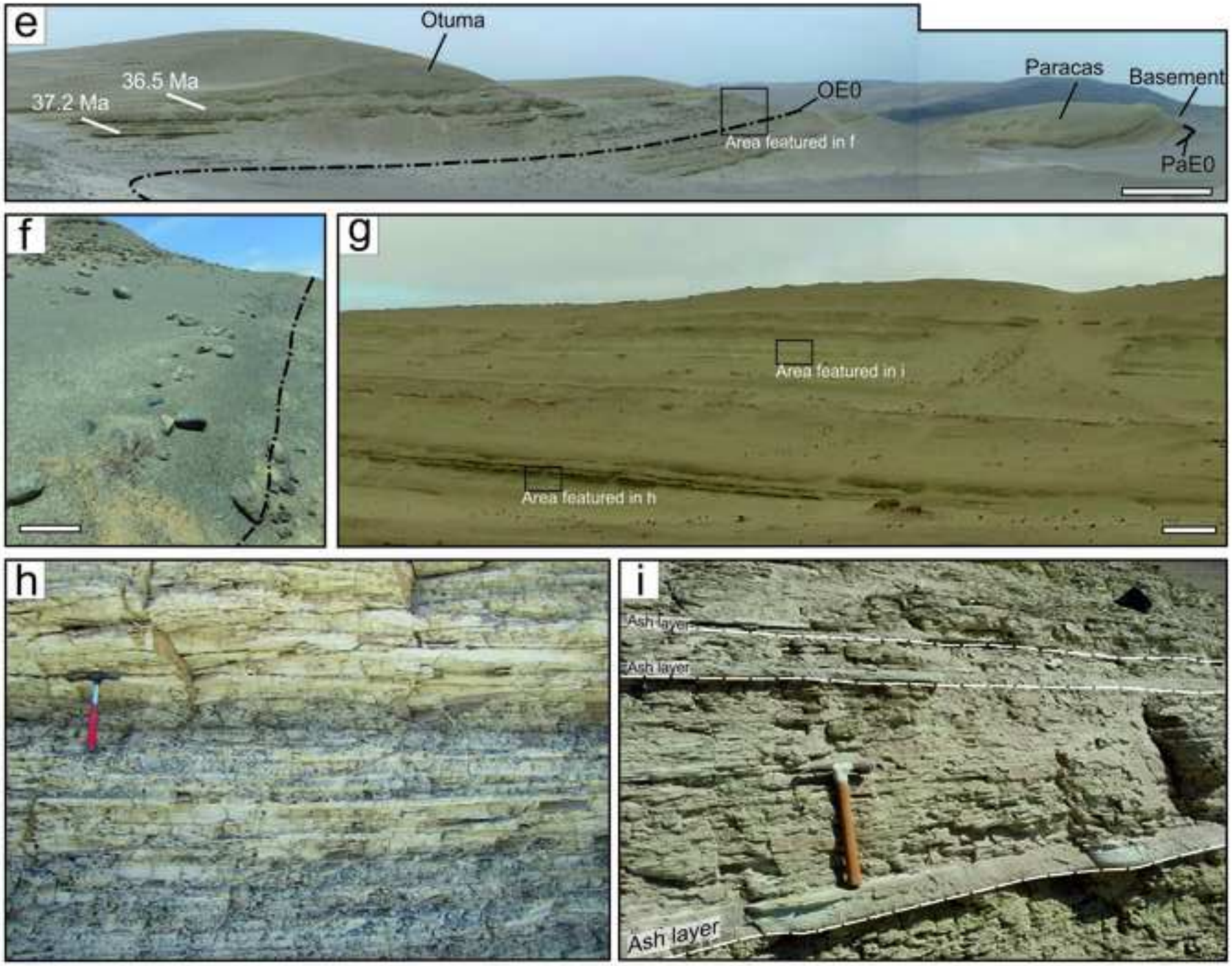

Figure 5

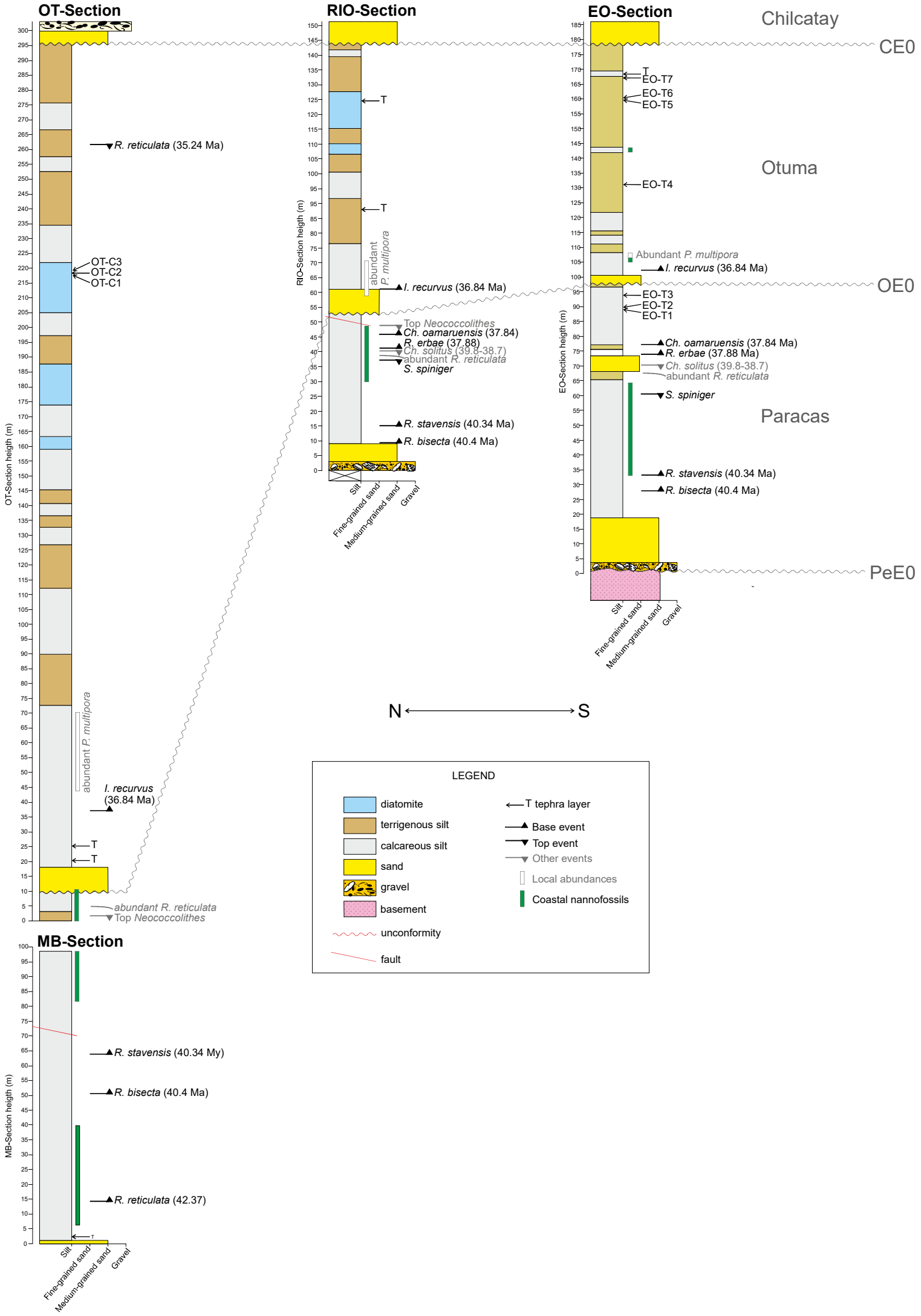

Figure 6

Click here to access/download;Figure;Figure6.tif

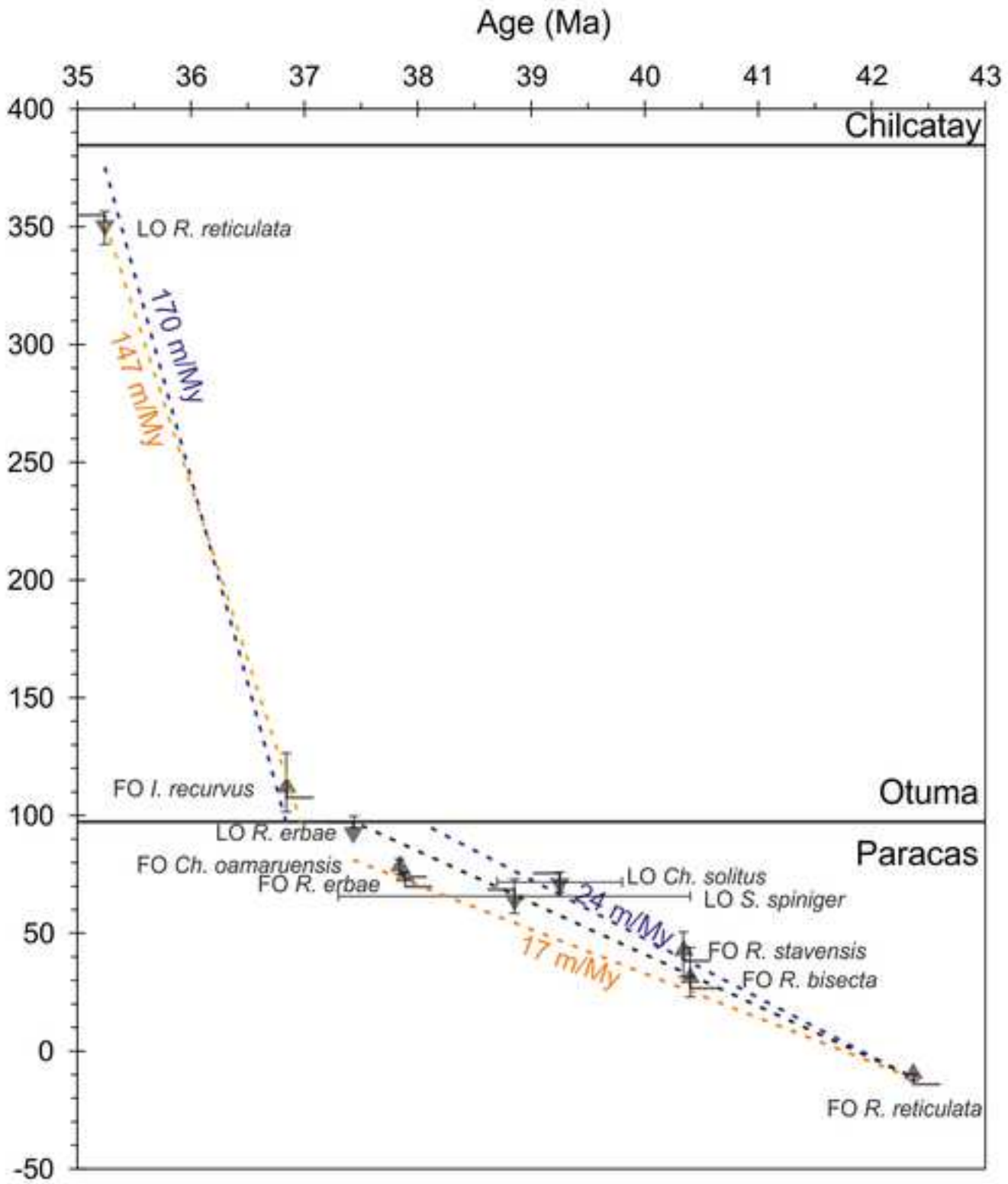

Figure 7

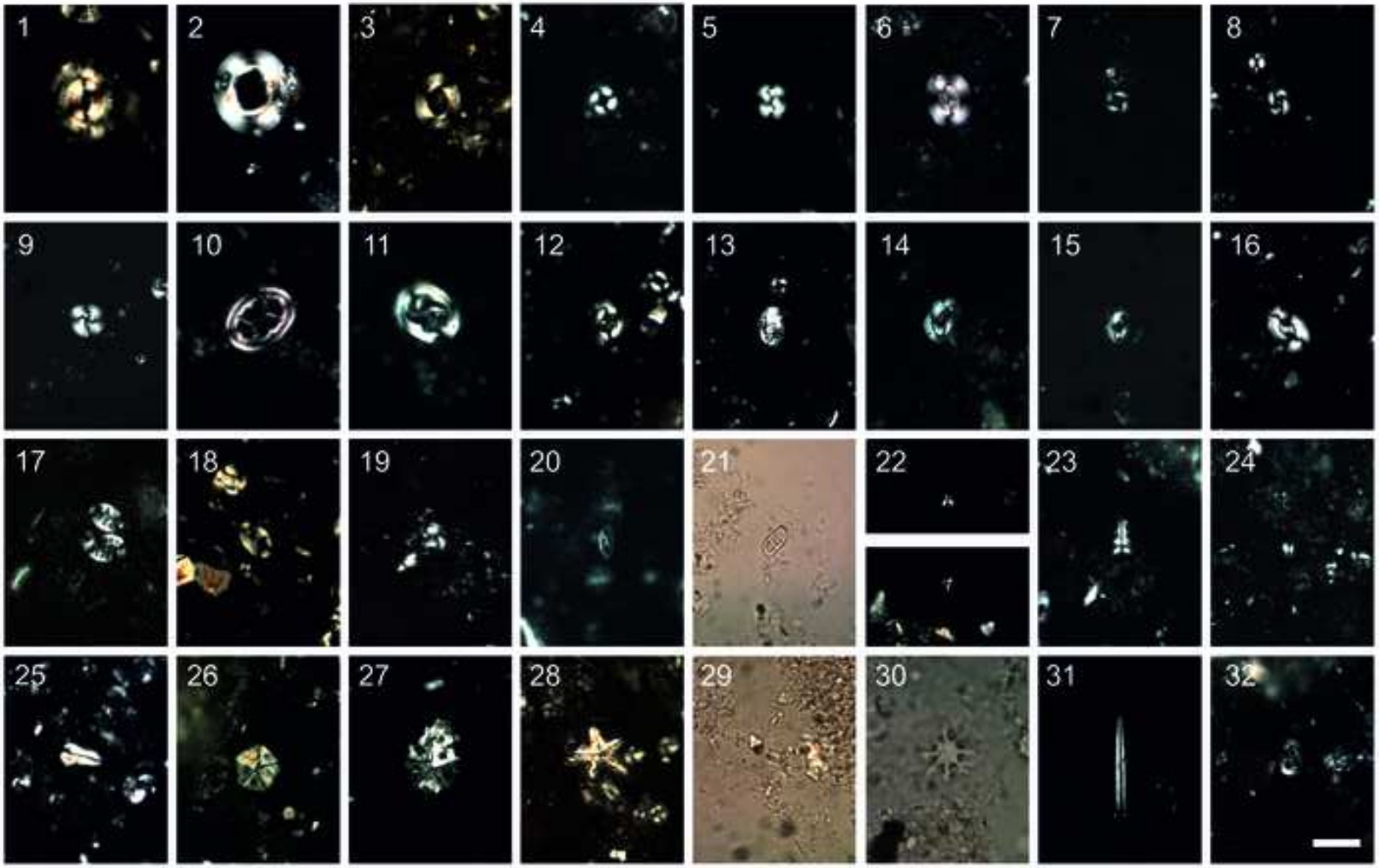

Figure 8

Click here to access/download;Figure;Figure8_contrasted.jpg

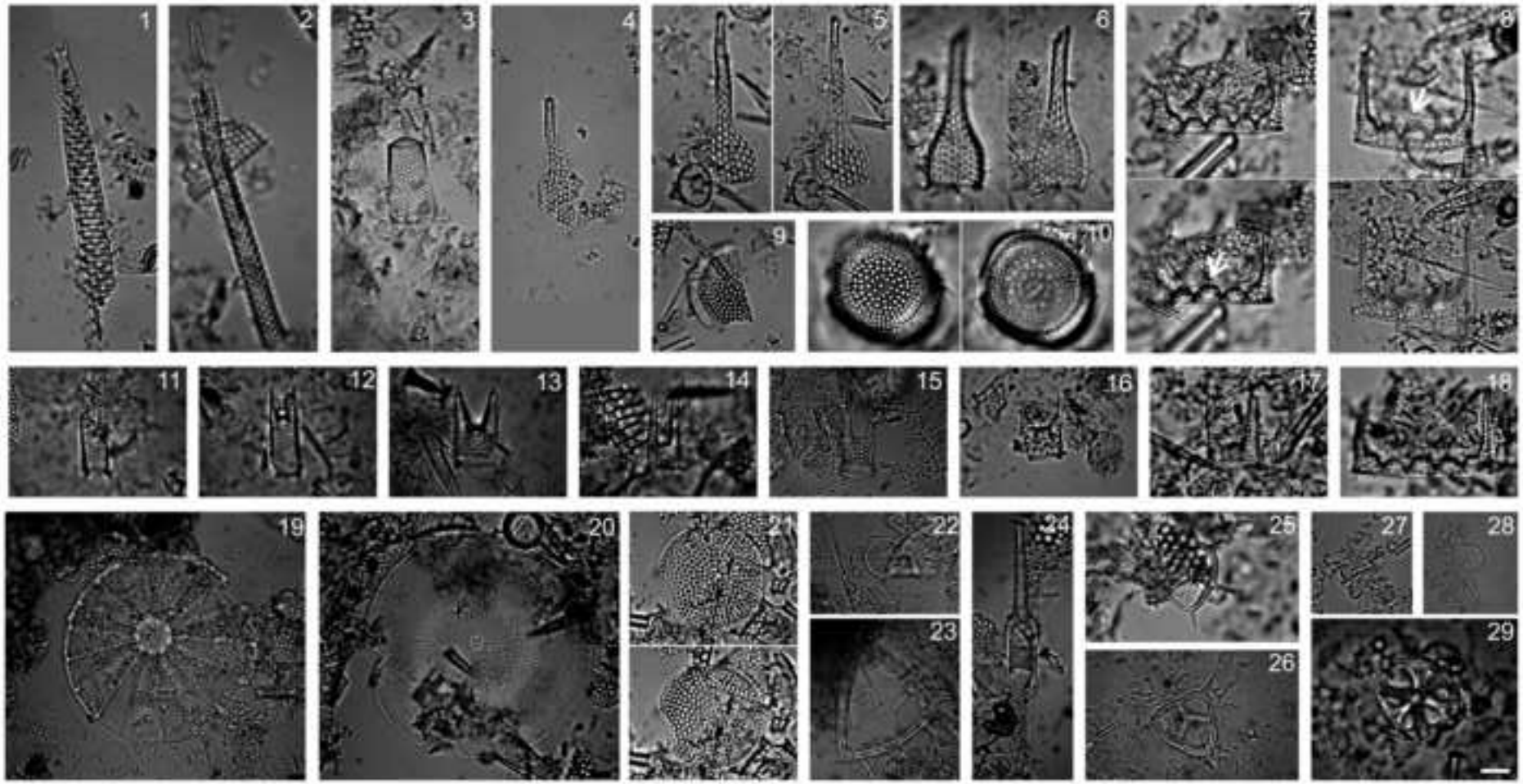

Declaration of interests for the paper

(Bio)stratigraphic overview and paleoclimatic-paleoceanographic implications of the middle-upper Eocene deposits from the Ica River Valley (East Pisco Basin, Peru)

by Elisa Malinverno, Giulia Bosio, Claudio Di Celma, Karen Gariboldi, Anna Gioncada, Pietro Paolo Pierantoni, Alberto Collareta, Giancarlo Molli, Gabriella Bagnoli, Giovanni Sarti, Mario Urbina, Giovanni Bianucci.

☒ The authors declare that they have no known competing financial interests or personal relationships that could have appeared to influence the work reported in this paper.

Figure A1

Figure A2

Figure A3

Click here to access/download

Supplementary Material

Appendix3_oldAppendix2.xlsx

Figure A4

(Bio)stratigraphic overview and paleoclimatic-paleoceanographic implications of the middle-upper Eocene deposits from the Ica River Valley (East Pisco Basin, Peru)

Elisa Malinverno[a]*, Giulia Bosio[a], Claudio Di Celma[b], Karen Gariboldi[c], Anna Gioncada[c], Pietro Paolo Pierantoni[b], Alberto Collareta[c], Giancarlo Molli[c], Gabriella Bagnoli[c], Giovanni Sarti[c], Mario Urbina[d], Giovanni Bianucci[c]

[a] Dipartimento di Scienze Dell'Ambiente e Della Terra, Università degli Studi di Milano-Bicocca, 20126, Milano, Italy.

[b] Scuola di Scienze e Tecnologie, Università di Camerino, 62032, Camerino, Italy

[c] Dipartimento di Scienze Della Terra, Università di Pisa, 56126, Pisa, Italy

[d] Departamento de Paleontología de Vertebrados, Museo de Historia Natural, Universidad Nacional Mayor de San Marcos, Lima 1, Peru

* corresponding author: Elisa Malinverno elisa.malinverno@unimib.it Piazza della Scienza, 4 – 20126 Milano (Italy)

Giulia Bosio: giulia.bosio@unimib.it

Claudio Di Celma: claudio.dicelma@unicam.it

Karen Gariboldi: karengariboldi@gmail.com

Anna Gioncada anna.gioncada@unipi.it

Alberto Collareta: alberto.collareta@unipi.it

Giancarlo Molli: giancarlo.molli@unipi.it

Giovanni Sarti: giovanni.sarti@unipi.it

Gabriella Bagnoli: gabriella.bagnoli@unipi.it

Pietro Paolo Pierantoni: pietropaolo.pierantoni@unicam.it

Mario Urbina: mariourbina01@hotmail.com

Giovanni Bianucci bianucci@dst.unipi.it

[1]

Abstract

The Eocene sediment successions of the East Pisco Basin (southern Peru) host an exceptionally rich and well-preserved assemblage of vertebrate fossils. However, due to the dearth of geochronological and biostratigraphic controls as well as of stratigraphic correlations, our understanding of these rocks and their fossil content remains elusive.

This paper provides a comprehensive calcareous nannofossil, diatom, and silicoflagellate biostratigraphic framework for the Eocene strata exposed at four localities along the Ica River Valley, permitting a robust chronological calibration of the marine vertebrate fauna entombed therein and a better definition of important appearance/ extinction events. The Paracas Formation, deposited directly on top of the Proterozoic and Paleozoic rocks of the crystalline basement, is formed by a siliciclastic-bioclastic gravel-sized deposit (Los Choros member) and calcareous-terrigenous siltstone (Yumaque member) that was deposited from the Lutetian (47.8-41.2 Ma) through the Bartonian (41.2-37.7 Ma) to the early Priabonian (37.7-33.9 Ma). The unconformably overlying Otuma Formation consists of a basal sand, followed by calcareous siltstone intercalated by diatomite layers towards the top. In the study area, the Otuma Formation is Priabonian in age and is truncated at the top by an unconformity at the base of the overlying Miocene Chilcatay Formation. Due to the angular nature of the unconformity, the upper Otuma strata reach the Oligocene elsewhere.

Average sedimentation rates range from 17 to 24 m/My in the Yumaque member of the Paracas Formation and increase to 147-170 m/My in the Otuma Formation. The microfossil assemblages witness a coastal setting with warm-temperate conditions for the Paracas Formation that become slightly cooler (though still temperate) in the upper Otuma Formation. Diatomaceous layers in the upper Otuma Formation indicate an overall increase in nutrient availability, which could reflect the global reorganization of ocean currents at

[1] m abs = meters above base of section
EOT = Eocene-Oligocene Transition
MECO = Middle Eocene Climatic Optimum

the Eocene-Oligocene transition. However, the taxonomic composition of the diatom assemblage suggests seasonal rather than persistent upwelling conditions.

Keywords

Paracas Formation, Otuma Formation, calcareous nannofossils, diatoms, silicoflagellates, fossil Lagerstätte

1. Introduction

The Eocene-Miocene deposits of the East Pisco Basin, southern Peru, feature exceptionally common and remarkably well-preserved marine vertebrate remains that make them a true Fossil Lagerstätte. Fossils from the East Pisco Basin include marine mammals, seabirds, marine reptiles, and fishes (Bianucci et al., 2016a; 2016b; 2016c 2018; 2020; Clarke et al., 2007; 2010; Collareta et al., 2015; 2017; 2020a; 2020b; de Muizon et al., 2019; Gioncada et al., 2016; 2018; Lambert et al., 2015; 2017a; 2017b; 2019; 2020a; 2020b; Landini et al., 2017a; 2017b; 2019; Marx et al., 2017).

The abundance of fossils and the stratigraphic continuity along a broad time interval make the sediment fill of the East Pisco Basin an ideal reservoir for reconstructing in detail the evolutionary trajectories of several marine vertebrate clades and to correlate them to the main abiotic events that, at regional and global scales, led to important changes in the ecological structure of the marine biota during the Cenozoic (Marx and Uhen, 2010; Norris et al., 2013).

In particular, the middle-late Eocene is one of the most critical phases of the Cenozoic Earth history, having involved deep structural changes in the overall geography of the global ocean and landmasses as well as in the climatic and oceanographic systems (Goldner et al., 2014; Lagabrielle et al., 2009). These abiotic changes promoted several dispersion events and the redistribution and partition of food resources, which, in turn, caused an increase in diversity and disparity of the marine vertebrates (Moore et al., 2014; Nilsen et al., 2003).

As such, the Eocene record of the East Pisco Basin is of key importance for unravelling the evolutionary history of the cetaceans as it allows for tracing the early phases of their worldwide dispersion with the first indisputable quadrupedal whale from the Pacific Ocean (Lambert et al., 2019), investigating the subsequent achievement of fully pelagic adaptations in the basilosaurids (Martínez-Cáceres and de Muizon, 2011; Martínez-Cáceres et al., 2017; Uhen et al., 2011) and highlighting the very origin of the "baleen" whale clade with the oldest known mysticete (de Muizon et al., 2019; Lambert et al., 2017b).

The Paleogene fossil record of the East Pisco Basin also documents two separate dispersals of penguins (Sphenisciformes) to the equatorial regions during greenhouse Earth conditions in the middle and late Eocene, i.e., significantly earlier than the recent most dispersal (ca 4-8 Ma) of penguins to the low latitudes (Clarke et al., 2007). Furthermore, an exceptionally well-preserved fossil of a giant-sized penguin found in upper Eocene deposits of the East Pisco Basin highlighted an early origin of the shape and colour of the feathers of these seabirds (Clarke et al., 2010). Not least, the recent description of an exquisitely preserved sawfish (Rhinopristiformes) from the middle Eocene of the Pisco Basin provides evidence for the first dispersal of pristids along the Pacific Coast of South America when the Peruvian nearshore waters were warmer than today due to a weaker upwelling regime (Collareta et al., 2020b).

The Paleogene strata from which these outstanding fossil records were obtained, have been described for some localities of the Pisco Basin and sparsely dated via ^{39}Ar-^{40}Ar dating (DeVries, 1998; Uhen et al., 2011), as well as by biostratigraphic data on their radiolarians, diatoms, calcareous nannofossils and foraminifera (Coletti et al., 2019; DeVries, 1998; DeVries et al., 2006; Dunbar et al., 1990; Fourtanier and Macharé, 1988; Ibaraki, 1993; Lambert et al., 2019; Lambert et al., 2017b; Macharé et al., 1988; Macharé and Fourtanier, 1988; Marty, 1989; Tsuchi et al., 1992; 1988). Nonetheless, a thorough biostratigraphic assessment of these sediment units is at present still lacking.

Our work aims at defining a high-resolution biostratigraphic framework for the Paleogene Paracas and Otuma Formations through the Zamaca area, some 50 km south of the town of Ica, based on the integration of calcareous nannofossil, diatom and silicoflagellate biostratigraphy from four measured stratigraphic sections along the Ica River Valley. Coupled with prior absolute ^{39}Ar-^{40}Ar ages, and compared with previous sparse dating at other localities, the herein presented stratigraphic scheme will support the

age determination of many marine vertebrate fossils that have been (and are being) collected from these formations, whose palaeontological content comprises one of the most globally representative marine vertebrate fossil assemblages for the middle-late Eocene time span.

2. Geological setting

2.1. Regional setting

The East Pisco Basin is one of the Cenozoic forearc basins developed along the coast of Peru and related to the subduction of the Farallon/Nazca plate underneath the South American plate (Thornburg and Kulm, 1981). Oblique subduction, extensional and strike-slip faults, as well as basal subduction erosion (Clift et al., 2003; von Huene and Lallemand, 1990; Herbozo et al., 2020) are responsible for a long-lasting and discontinuous subsidence that continued from the Eocene to the Mio-Pliocene, providing the accommodation space for the deposition of a thick sedimentary succession.

Structural highs of different nature, running almost parallel to the coast, separate two sets of basins. From north to south, the shelf Sechura, Salaverry and East Pisco basins are bound by the Coastal Batholith onshore and the Outer Shelf High offshore, while several slope basins, including the Talara, Truillo, Yaquina, Lima, West Pisco, and Caballas basins (Suess andVon Huene, 1988), occur between the Outer Shelf High and the Upper slope Ridge offshore (Figure 1a).

2.2. The East Pisco Basin

The Cenozoic sediment infill of the East Pisco Basin (Figure 1b) lays on a basement comprising the Proterozoic Arequipa Massif (Ramos, 2008 and references therein) intruded by the lower Paleozoic granitoids of the San Nicolás batholith (Musaka and Henry, 1990) and overlain by the Jurassic volcanosedimentary rocks of the Guaneros Formation (Léon et al., 2008) and is punctuated by a series of conspicuous erosional unconformities that bound sedimentary units on a variety of scales (DeVries, 1998;

Dunbar et al., 1990; Di Celma et al., 2018a, 2019). The oldest unit encountered in the basin fill-succession, assigned to the Ypresian, was described near Puerto Caballas by DeVries (2017) and is of continental and marginal marine nature (DeVries, 2019); this unit is not present in our study area.

The Paracas Formation, as described by Dunbar et al. (1990) in the study area rests directly on the crystalline basement and comprises two lithostratigraphic units: the middle Eocene coarse-grained biogenic Los Choros member (Balarezo et al., 1980; Petersen, 1954) and the middle-upper Eocene fine-grained Yumaque member. The Otuma Formation, as originally defined by DeVries (1998) in the Paracas Peninsula, is a fine-grained unit that was originally dated to the early Oligocene. Its base however was subsequently redefined in our study area and constrained by Ar-Ar data to the late Eocene (DeVries et al., 2006; DeVries et al., 2017). The Chilcatay Formation is composed of mixed coarse- and fine-grained successions recording deposition in shoreface, offshore, and subaqueous delta settings. An internal unconformity separates this unit into two distinct stratal packages, namely Ct1 and Ct2. It was deposited between the late Oligocene-early Miocene (Macharé et al., 1988) but only lower Miocene deposits have been reported from our study area so far (Di Celma et al., 2018b; Di Celma et al., 2019; Lambert et al., 2017a). The Pisco Formation is an extended sedimentary unit, constituted by three distinct unconformity-bounded stratal packages, named P0, P1 and P2 (Di Celma et al., 2017; Di Celma et al., 2018a; Di Celma et al., 2016a; Di Celma et al., 2016b). Each of these units consists of a basal boulder layer with phosphate nodules and containing abundant mollusks, followed by a sandy interval that passes upwards into a thick succession of silt-grade sediments. While terrigenous siltstones are dominant in P0, diatomites occur in P1 and P2. The age of the three sequences have been constrained through a combination of ^{39}Ar-^{40}Ar dating, strontium isotopic ($^{87}Sr/^{86}Sr$) estimates and diatom biostratigraphy (Bosio et al., 2018; Bosio et al., 2020a; Bosio et al., 2020b; Gariboldi et al., 2017) between 14.8–12.4 Ma (P0), 9.5-8.6 Ma (P1) and 8.4-6.7 Ma (or younger, P2). Pliocene strata of the Pisco Formation have also been documented near the city of Pisco, about 170 km northwest of the current study area (Solís Mundaca, 2018).

2.3. Nature and age of upper Paleogene sediments of the East Pisco Basin and other Peruvian forearc basins

Sedimentation in the forearc basins of Peru has occurred since the Eocene and is represented by different sediment types. Throughout the coastal outcrops of Peru, the lower Eocene is characterised by continental deposition, documented from north (Talara Basin, Higley, 2004) to south (Caballas basin, DeVries, 2017). In the Talara basin, lower Eocene shallow marine deposits (Mogollon Formation, Narvàez-Rodriguez and Pardo-Arguedas, 2009) are followed by middle-upper Eocene deeper water deposits of the Talara group, which have been dated through nannofossil biostratigraphy (CP12-15; NP14-20, Narvàez-Rodriguez and Pardo-Arguedas, 2009; Narvàez-Rodriguez and Setembrino, 2001).

The Paracas Formation comprises the oldest sediments exposed in the studied portion of the East Pisco Basin (Figure 2, 3). They are Lutetian in age and consist of coarse-grained biogenic limestones of the Los Choros member at the base (e.g. Coletti et al., 2019; DeVries, 1998; Dunbar et al., 1990; Léon et al., 2008; Lisson, 1925; Rivera, 1957), grading upward into Lutetian-Priabonian calcareous and terrigenous sediments of the Yumaque member, that in turn are overlain by the Otuma Formation (DeVries, 1998; Dunbar et al., 1990).

Eocene laminated diatomites occur in the East Pisco Basin and were dated through radiolarian (Dunbar et al., 1990; Marty et al., 1988) and diatom (Fourtanier and Macharé, 1988) biostratigraphy to the late Eocene, with a minimum age datum to the lower Oligocene at Fundo Desbarrancado (Figure 2). They were originally assigned to the Yumaque member of the Paracas Formation but now considered as part of the Otuma formation, as recently redefined by DeVries et al. (2006; 2017) in the Ica River Valley. Radiolarian-rich diatomites have been reported from different locations of the East Pisco Basin, from north to south: Playa Yumaque, Quebrada Perdida, Quebrada Santa Cruz (Dunbar et al., 1990; Fourtanier and Macharé, 1988; Marty et al., 1988) and from the Chira Formation in the Sechura Basin at Bahovar (Dunbar et al., 1990). Planktonic foraminifera biostratigraphy of the sedimentary sections in the northern sector of the East Pisco Basin revealed a middle Eocene age for sandstone-siltstones exposed near the city of Paracas and an early Oligocene age for sandstones exposed at Playa Yumaque and Salinas de Otuma (Ibaraki, 1993). The latter sections were subsequently used by DeVries (1998) to define the transgressive Oligocene Otuma Formation (32-31 Ma), above the middle-upper Eocene Yumaque Formation (42-34 Ma). The two units are

separated by an unconformity, marked by a mixture of crystalline boulders from the basement and oysters, interpreted as due to local tectonics and possibly diachronous across the East Pisco Basin (DeVries, 1998). Re-visitation of outcrops and new age determinations at different localities of the East Pisco Basin (DeVries et al., 2006; 2017) led to the definition of a late Eocene-early Oligocene age for the Otuma Formation in the East Pisco Basin. Therefore the diatomaceous layers, previously assigned to the directly underlying Yumaque member of the Paracas Formation, are now part of the Otuma Formation. Dating of the Chira Formation in the Sechura Basin also provided a late middle-late Eocene age from radiolarians (Dunbar et al., 1990) as well as from calcareous nannofossils and diatoms (NP 17-20, Tsuchi et al., 1988). Middle-upper Eocene marine sediments were recovered through ocean drilling off the Peruvian coast, but only at some sites on the lower slope of the forearc (ODP112-683, seaward side of Yaquina Basin to the north, ODP112-682, 688 to the south, Martini, 1990a) and on the Nazca Plate offshore (DSDP 34-321 and ODP201-1231, Blechschmidt, 1976) and not on the shelf – upper slope basin, with one exception (Delfin well, Tuijllo Basin,) where coarse-grained sandstones and shales-limestones of shallow marine environment (Prudhomme et al., 2019 and references therein) were present, followed by diatomites (Schrader and Castaneda, 1990).

3. Methods

3.1. Field work and sample collection

A detailed investigation of the Paracas and Otuma strata exposed along the Ica River Valley (Figure 1a; 2) was carried out in the Zamaca area between 2016 and 2019. Due to the lithological similarity of most formations of the East Pisco Basin (DeVries, 1998) and the presence of several faults that complicate the three-dimensional architecture of the basin fill, identification and correlation of the different formations in the field was often complex and required careful recognition and detailed geological mapping.

Four highly detailed stratigraphic columns, informally labelled EO-Section, RIO-Section, MB-Section, OT-Section, were logged through the strata of the Paracas and Otuma formations on both sides of the Ica River

and tens of reconnaissance locations were investigated, concentrating on an area of approximately 75 km^2 (Figure 2 4). Locations for logging of stratigraphic sections were selected based on quality of exposure, accessibility, and degree of faulting.

All stratigraphic sections were measured at a decimetre scale using a Jacob's staff and sediment samples for biostratigraphic purposes were collected 1.5 to 3 m apart while measuring the sections. Furthermore, an additional 10 m thick stratigraphic column (ZAN-Section, base: 14°38'2.7"S - 75°37'57.3"W; top: 14°38'2.1"S - 75°37'58.5"W) was measured in the northern portion of the study area at the top of the Otuma Formation up to the contact with the overlying Chilcatay strata and two samples were collected 50 cm and 1 m above an ash bed (ZAMA-32 and 33, respectively, 14°38'44.1''S - 75°38'11.4''W) corresponding to a previously-dated volcanic ash layer (87DV 508 1Snee of DeVries, 1998). The latter locations are shown in Figure 2. A north-south striking stratigraphic panel (Figure 5) used for correlation between outcrops from equivalent stratigraphic sections at different locations was compiled by hanging the sections from a young contact that is used as a horizontal stratigraphic datum (base of Chilcatay Formation).

According to previous studies (DeVries, 1998; DeVries, 2017; Dunbar et al., 1990), the different formations defined in the East Pisco Basin are separated by regional-scale major unconformities. In the field, unconformities were recognized as angular contacts and/or basal boulder layers within each measured section, walked with a hand-held GPS and traced on Google Earth images across the investigated area, wherever possible (Figures 2, 4, 5).

In order to further subdivide the formations, local marker beds whose lateral extension throughout the study area allowed good control on correlation have been identified, physically tracked and mapped. They mainly consist of decimetre-thick indurated layers that can also be identified in high-resolution Goole Earth images.

3.2. Biostratigraphy

All sediment samples were prepared with the standard smear slide method, using a 22x40 mm cover slip and Norland@ mounting medium. All samples were analysed with a BX50 light microscope at

1000x with immersion oil, considering at least two longitudinal transects or, in case of low abundances, the whole slide. Additional slides were prepared for diatom assessment, in order to detect rare marker taxa.

The presence and relative abundance of calcareous nannofossils, diatoms and silicoflagellates (Figure 7, 8) was assessed for each sample and tabulated (Figure A.1). The total abundance of each group relative to the remaining sediment was estimated using the categories of Koç and Scherer (1996): D = dominant, >60%; A = abundant, 20-60%; C = common, 5-20%; F = few, 2-5%; R = rare, <2%; B = barren.

Within each group, the relative abundance of each species was estimated per field of view (FOV) or transect on the slide, as: A = abundant; >10/FOV; C = common; 1–10 /FOV; F = few; 1/10 FOVs; R = rare; ≥ 3 /transect; VR = 1 /transect; Fragments (for diatoms, presence of broken valves); B = barren.

Preservation was indicated as: G = good, no evident sign of dissolution (nannofossils) or breakage (diatoms); M = moderate, signs of dissolution present but features still visible (nannofossils), common areolae enlargement and dissolution of frustule rims (diatoms); B = bad, strong signs of dissolution, features poorly preserved but species still recognizable (nannofossils); strong dissolution and breakage (diatoms); VB = very bad, nannofossil species undefined.

Calcareous nannofossil species follow the taxonomy of Perch-Nielsen (1985a) and Young et al. (2020). Zonal schemes are based on Martini (1971), with zonal codes NP, and on Agnini et al. (2014), with zonal codes CNE. Reference to the zonal scheme of Okada and Bukry (1980), with zonal codes CP is also made. All calibrated bioevents reported in Agnini et al. (2014) and recognised in the present work (Figure A.2, A.3) were used to build the age model (Figure A.4, Figure 6). All zonal schemes and relative bioevents were plotted with Time Scale Creator and referred to the Geomagnetic Polarity Time Scale 2020 of Gradstein et al. (2020) (Figure 3).

Diatom species follow an extended taxonomy (Fenner, 1984; Fenner, 1985; Gombos, 1976; Harwood and Bohaty, 2001; Oreshkina and Radionova, 2014; Strelnikova et al., 2001). The single species biostratigraphic range are reported by different authors (Arney et al., 2003; Barron, 1985; Barron and Baldauf, 1995; Barron et al., 1984; Barron et al., 2014; Barron et al., 2015; Danelian et al., 2007; Expedition 320/321 Scientists, 2010; Fenner, 1976; Fenner, 1984; Fenner, 1985; Gladenkov, 2013; Gombos, 1976; Lazarus et al., 2014; Oreshkina and Aleksandrova, 2007; Scherer et al., 2007; Sims et al., 1989; Strelnikova et al., 2001). We follow the

biozonal scheme of Barron et al. (2015), which was developed after the low-latitude zonation of Fenner (1984, 1985) and Scherer et al. (2007), including bioevents from Expedition 320/321 Scientists (2010). Silicoflagellate species follow the taxonomy developed during DSDP-ODP expeditions and summarised in Perch-Nielsen (1985b). The zonation of Bukry (1981), partly updated by Barron et al. (2015) is used. Ebridian and incertae sedis species follow Onodera and Takahashi (2009) and Witkowski et al. (2020).

3.3. Age model

The age model developed here for the upper Paracas-Otuma succession is based on calcareous nannofossil bioevents and is supported by diatom and silicoflagellate assemblages. The four investigated sections were correlated in the field and on Google Earth imagery using lithological marker layers (Figure 4, 5): from northwest to southeast, the base of the Otuma Formation (OE0 unconformity) and the base of the Chilcatay Formation (CE0 unconformity) are tracked through the OT, RIO and EO sections; the base of the Paracas (PaE0 unconformity) is tracked from the MB to the RIO and OT sections. As all the identified bioevents can be tracked from section to section (Figure 5), a composite section was created by aligning all sections at the base of the Otuma Formation and plotting bioevents on EO-section height (Table A.2). To do so:

- for the RIO-Section, the height has been adjusted due to the presence of a small-displacement normal fault close to the base of the Otuma Formation: for the Paracas Formation, the youngest bioevent (First Occurrence of *C. oamaruensis*) was correlated with the EO-Section; for the upper part of the RIO-Section, 15.5 m were added to account for the portion lost due to fault displacement, as estimated both in the field and through Google Earth images.
- For the MB-Section, which falls entirely in the Paracas Formation, the youngest bioevent (First Occurrence of *R. stavensis*) was correlated with that of the EO-Section and considering a certain distance of its top from the base of the overlying OT-Section: plotted in this way, the base of the MB-Section has an EO-Section scale height of -23 m, accounting for the basal portion of the sequence, which is not recorded at the EO-Section.

The age model (Figure 6) was created by averaging the height of bioevents among sections and considering vertical error bars (Figure A.2). Sedimentation rates were calculated for the Paracas and Otuma Formations considering different lines of correlation. Age-height plots and lines of correlations for the single stratigraphic sections are shown in Figure A.4.

4. Results

The lithology and biostratigraphy of the different stratigraphic columns (Figure 5; Figure A.1) is described below, from south to north. Heights are indicated as meters (m) above the base of the sections (abs).

4.1. The EO-Section

The EO-Section (Figure 4a) starts on the PaE0 unconformity, with a boulder layer on top of the crystalline basement, followed by about 17 m of medium-grained sand. This interval is barren of planktonic microfossils and represents the coarser Los Choros member of the Paracas Formation. This grades upward into the finer Yumaque member, characterised from 19 to 68 m abs by a slightly calcareous silt, with rare to very rare calcareous nannofossils that generally show a poor to very poor preservation. *Reticulofenestra reticulata* (base 42.37 Ma) is present from the base of this interval, pointing to a late LutetianBartonian age (biozones CNE14, upper NP16); its concentration is low but increases from 68 m abs upwards. *Reticulofenestra bisecta* and *Reticulofenestra stavensis* (base 40.34 Ma) occur at 24 and 34 m abs, respectively, indicating the base of CNE15. *Sphenolithus spiniger* is rare in the samples, and its last occurrence is observed at 61 m abs. Sphenoliths are overall rare in the samples, so neither the last occurrence of *S. furcatulithoides* nor the first occurrence of *S. obtusus* could be identified along the section. The last occurrence of *Chiasmolithus solitus* (FO between 39.8 and 38.7 Ma, marking the base of NP17) is observed at 70 m abs. *R. erbae* (FO at 37.88 Ma, LO at 37.46 Ma) and *C. oamaruensis* (FO at 37.84 Ma), two important markers for the Priabonian, are very rare in the samples, but their first occurrences were detected at 75 and 78 m abs, respectively, while the last occurrence of *R. erbae* occurred at the Paracas-

Otuma boundary. *Chiasmolithus grandis* is rare and scattered. Differently from the calibration of Agnini et al. (2014), its last occurrence is detected well below that of *C. solitus* and it is therefore not considered to build the age model.

Typical shallow water calcareous nannofossils (*Pemma basquense*, *Zygrhablithus bijugatus*) occur from 33 to 64 m abs. Three tephra layers occur in the 90-95 m interval.

At 98 m abs, the sharp OE0 unconformity (Figure 4a) marks the base of the Otuma Formation. This starts with 25 m of fine-grained sand, where calcareous nannofossils range from very rare to common and their preservation from very poor to moderate. The first occurrence of *Isthmolithus recurvus* (Base at 36.84 Ma, within CNE18 and marking the base of NP19-20), is detected 5 m from the base of the Otuma Formation within the fine sand at 103 m abs. An increase in abundance of *Pontosphaera multipora* is observed just above it at 106 m abs, representing a local correlation event. From 123 to 178.5 m abs, the lithology is represented by silt with a dominant terrigenous composition and the presence of five tephra layers and several indurated (carbonate) orange layers. Calcareous nannofossils are absent or very rare, preventing the identification of any bio-event. The highest sample in the section that contains calcareous nannofossils is at 169 m abs: *R. reticulata* is still present, pointing to a late Priabonian age (CNE19 or 20 and NP19-20). The sediments of the Otuma Formation do not contain diatomaceous layers and are truncated at the top by the CE0 unconformity, followed by the coarse sand layers of the overlying Chilcatay Formation.

4.2. The RIO-Section

The RIO-Section (Figure 4b) starts a few meters above the PaE0 unconformity, with 9 m of gravel grading upward into medium-grained sand: these represent the coarse-grained Los Choros member of the Paracas Formation. This interval is followed by 44 m of slightly calcareous silt, constituting the finer Yumaque member of the Paracas Formation. Calcareous nannofossils are present from 7 m abs upward, ranging from very rare to common and with moderate to bad (good in one sample) preservation. *R. reticulata* is present, although rare, from 7 m abs and becomes common from 39 m upwards. *Reticulofenestra bisecta* and *R. stavensis* occur at 9 and 15 m abs, respectively, pointing to the base of biozone CNE15.

Sphenolithus spiniger is rare and scattered and only occurs up to 37 m abs. No other stratigraphically useful sphenoliths were recovered. Probably due to the lower sampling resolution (3 m), the last occurrence of *C. solitus* and the first occurrence of *R. erbae*, separated by almost 1 Ma, were both detected at 41 m abs and the first occurrence of *C. oamaruensis* was detected at 46 m abs. *Chiasmolithus grandis* is scattered throughout the section and its last occurrence is detected at 33 m abs, below that of *C. solitus*. *Neococcolithes* spp., indicated by some authors to indicate the Bartonian/Priabonian limit, are scattered in the lower samples and last occur at 49 m abs. Typical shallow water calcareous nannofossils (*Pemma basquense*, *Zygrhablithus bijugatus* and *Micrantholithus* spp.) occur from 30 to 49 m abs.

At 50 m abs, the section is truncated by a normal fault that, due to sediment cover, was not detected during the field work, but was later observed from Google Earth imagery. The thickness of the sediment column lost by fault dislocation was estimated to be approximately 15.5 m.

The sharp OE0 unconformity (Figure 4b) at 53 m marks the base of the Otuma Formation. This is characterised by about 8 m of fine-grained sand, followed by 82 m of slightly calcareous silt: this becomes predominantly terrigenous silt upwards and, towards the top, two diatomacous layers (106.5-110 m abs and 115-127.5 m abs) are present. Several cemented (carbonate) orange layers occur along the sediment column, some of them forming distinct benches in the field, and two tephra layers were identified (at 88 and 125 m abs). In the non-barren layers, calcareous nannofossils range from very rare to common and their degree of preservation is very poor to good. *Isthmolithus recurvus* appears at 61.5 m abs just above the basal fine-sand layer (marking the base of NP19-20). An increase in *P. multipora* is observed from 57 to 69 m abs. No further calcareous nannofossil bioevents were recorded above, due to the absence of calcareous nannofossils or their bad preservation. The highest sample in the section that contains calcareous nannofossils is at 98 m abs: *R. reticulata* is still present, pointing to a late Priabonian age (CNE19 or 20 and NP19-20).

Diatomites are characterised by a diverse diatom assemblage (Figure A.1) with some markers (Figure A.3) typical of the late Paleocene to middle Miocene (*Hemiaulus altus*), Eocene to early Miocene (*Distephanosira architecturalis*), late Paleocene to late Eocene (*H. subacutus* without basal constrictions, Fenner, 1985), Eocene to late Oligocene (*Pyxilla gracilis*), middle Eocene to early Oligocene (*H.*

polycystinorum, P. reticulata). *Cestodiscus* is rare to few and mostly represented by the late Eocene *Cestodiscus* aff. *intersectus*, with rare occurrences of the middle-late Eocene *C. senarius* and the marker species *C. pulchellus* var. *novazealandica* (FO 39.0 Ma, LO 35.0 Ma) and *C. fennerae* (FO 36.9 Ma, LO 34.1 Ma). *Azpeitia tuberculata-oligocenica*, a transitional form (Barron pers. comm.) restricted between the late middle Eocene and late Eocene (Barron et al., 2014) also occurs. Therefore, the diatomaceous portion of the stratigraphic section can be assigned to the *Cestodiscus fennerae* zone.

Silicoflagellates are represented by rare specimens of *Corbisema triacantha* s.l. and the middle-late Eocene marker *Dictyocha hexacantha* (*D. hexacantha* zone, e.g. Perch-Nielsen, (1985b), correlated with nannofossil zone CP13c-CP15a (Barron et al., 1984) with last occurrence at 36.6 Ma, Barron et al., 2015), thus supporting a late Eocene age for this portion of the section. Rare occurrences of the ebridian *Ebriopsis crenulata* (middle Eocene-Oligocene) are observed.

The section is truncated at the top by the CE0 unconformity, marking the base of the overlying Chilcatay Formation

4.3. The MB-Section

The MB-Section (Figure 4c) starts a few metres above the crystalline basement, with 1 m of fine-grained sand, representing the top of the coarser Los Choros member of the Paracas Formation and is followed by 98 m of slightly calcareous silt of the finer Yumaque member. Excluding a few barren samples, calcareous nannofossils range from very rare to common and their preservation is poor to moderate or even good. The first occurrence of *R. reticulata* (42.37 Ma) is identified at 15 m abs, indicating the base of CNE14. *R. reticulata* ranges from rare to few throughout the section. *R. bisecta* and *R. stavensis* (Base at 40.34 Ma) occur at 50 and 64 m abs, respectively, marking the base of CNE15. Additional bio-events were not detected along this section and *S. spiniger* and *C. solitus* are still present at the top. Typical shallow water calcareous nannofossils (*Pemma basquense*, *Zygrhablithus bijugatus* and *Micrantholithus* spp.) occur from 6 to 40 m abs and from 82 m abs to the top of the section.

4.4. The OT-Section

The OT-Section (Figure 4d) is the continuation of the MB-Section at a slightly northern location. This section is a composite of five partial sections pieced together by walking along indurated orange layers connecting the stratigraphically upper part of one exposure to the lower part of a nearby exposure. The section starts with 10 m of fine silt of the Yumaque member of the Paracas Formation containing abundant *R. reticulata* and rare specimens of *Neococcolithes* at the base. The sharp OE0 unconformity, characterised by a boulder layer (Figure 4e and 4f), marks the base of the Otuma Formation, that starts with 8 m of medium-grained sand, followed by 277 m of silt, characterised by a slightly calcareous composition (Figure 4h) at the base but becoming mostly terrigenous upwards; diatomites are present at 149-152, 164-176 and 195-212 m abs. Three tephra layers occur within the 217-220 m abs layer (Figure 4i). Several cemented (carbonate) orange layers occur along the section and form distinct layers, that have been traced for correlation purposes (Figure 2 and 4d).

In the non-barren layers, calcareous nannofossils range from very rare to common and their preservation is very poor to moderate. *S. spiniger*, *C. solitus*, *R. erbae* and *C. oamaruensis* were not detected, so the last occurrence of the first two and the first occurrence of the latter two must be at some point between the top of the MB-Section and the base of the OT-Section. *Isthmolithus recurvus* (Base at 36.84 Ma, within CNE18 and at the base of NP19-20) appears at 37 m abs and is followed by increased abundance of *P. multipora* from 44 to 71 m abs. Zone CNE19 was not identified. The last occurrence of *R. reticulata* was detected at 257 m abs and marks the base of CNE20. *D. saipanensis* and *D. barbadiensis* are still present in the uppermost nannofossil-containing samples at 273 m.

Diatomites contain an abundant and diverse diatom assemblage with some markers typical of the late Paleocene to middle Miocene (*H. altus*), late Paleocene to late Eocene (*H. subacutus* without basal constrictions, Fenner 1985), Eocene to early Miocene (*D. architecturalis*), Eocene to late Oligocene (*P. gracilis*), middle Eocene to early Oligocene (*H. polycystinorum*, *P. reticulata*). Furthermore, in the uppermost sample (OT63), we found also one specimen of *H. subacutus* with basal constrictions typical of early Oligocene specimens (Fenner, 1985) and a few specimens of the middle-late Eocene species *H. grassus* (LO 35.1 Ma Expedition 320/321 scientists, 2010). Rare to few late Eocene *Cestodiscus* aff. *intersectus*, rare middle-late Eocene *C. senarius*, rare *C. pulchellus* var. *novazealandica* (FO 39.0 Ma – LO

35.0 Ma) and late middle Eocene to late Eocene *A. tuberculata-oligocenica*. Therefore, the upper diatomaceous portion of the stratigraphic section can be assigned to the *Cestodiscus pulchellus* var. *novazealandica* – *C.fennerae* zone.

Silicoflagellates are rare in these samples, but represented by a typical Eocene species, *N. foliacea*, as well as the middle-late Eocene marker, *Dictyocha hexacantha*. This species is absent from the topmost sample (OT63), where a few specimens of the late late Eocene to Oligocene *C. triacantha mediana* were identified. Rare occurrences of the ebridian *E. crenulata* (middle Eocene to Oligocene) and of the incertae sedis *M. barbadensis* (middle Eocene to early Oligocene) are observed.

At 296 m abs, the Otuma Formation is truncated at the top by the CE0 unconformity, followed by the coarse sand layers of the overlying Chilcatay Formation.

4.5. Additional samples

The 10 m thick ZAN-Section (not drawn) has been sampled within the upper Otuma layers up to the contact with the overlying Chilcatay Formation and consists mainly of terrigenous silt. Calcareous nannofossils are only present in three samples, where they are few to common in abundance and with a moderate to poor preservation. The assemblage is depleted and is mainly represented by large placoliths (*R. bisecta*, *R. stavensis*, *C. formosus*, *C. pelagicus*); *R. reticulata* was never observed, while *D. saipanensis* was present in one sample, thus assigning this interval to biozone CNE20.

Diatom fragments were present in the upper portion of the sequence, but no intact valves have been observed.

The two ZAMA samples, obtained from just above one of the tephra layers dated in DeVries (1998) at 35.7 Ma, are represented by diatomites, while calcareous nannofossils are absent. Diatom assemblages contain some markers typical of the Paleocene to the early Oligocene (*Pterotecha aculeifera*), late Paleocene to late Eocene (*Hemiaulus subacutus* without basal constrictions, Fenner, 1985), late Paleocene to middle Miocene (*H. altus*), Eocene to early Miocene (*D. architecturalis*), middle Eocene to early Oligocene (*H. polycystinorum*). Rare late Eocene *Cestodiscus* aff. *intersectus*, very rare middle-late Eocene *Cestodiscus senarius*, very rare *Cestodiscus pulchellus* var. *novazealandica* (FO 39.0 Ma – LO 35.0 Ma) and late middle –

late Eocene *Azpeitia tuberculata-oligocenica* also occur. Therefore, the upper diatomaceous portion of the stratigraphic section can be assigned to the *Cestodiscus pulchellus* var. *novazealandica* – *C. fennerae* zone. Silicoflagellates are few but diverse and contain *Dictyocha hexacantha* (Middle-Late Eocene), *Corbisema triacantha* s.l., *Corbisema jerseyensis*, indicated as a late Eocene species (Barron et al., 2014; Bukry, 1987; Tsoy, 2011), *Corbisema hastata incohata*, common from late Eocene sediments (Bukry, 1987), *Naviculopsis foliacea*, spanning the whole Eocene with rare specimens found in the early Oligocene (McCartney et al., 2020) and *Bachmannocena apiculata* typical of the late Eocene-early Oligocene (Hajós, 1976). Long-ranging *Stephanocha speculum* and *Distephanopsis crux* were observed only in a few samples.

5. Discussion

5.1. Eocene biostratigraphic markers in the East Pisco Basin and local correlation events

Although several biostratigraphic studies have been performed for the East Pisco Basin Eocene sediments, by means of calcareous nannofossils, diatoms, planktonic foraminifera and radiolarians (Fourtanier and Macharé, 1988; Macharé and Fourtanier, 1988; Tsuchi et al., 1992; Tsuchi et al., 1988; Ibaraki et al., 1993; DeVries, 1998), and often resulting in the recognition of biozones, only a few stratigraphic columns have been analysed in detail, with the identification of bioevents. Among these, Lambert et al. (2017b, 2019) dated through calcareous nannofossils a stratigraphic column across the Paracas and Otuma formations at the locality of Media Luna. Coletti et al. (2019) dated through benthic foraminifera the uppermost portion of the Los Choros member and through calcareous nannofossils the basal layers of the Yumaque member along a short section across the Ica River Valley. Marty (1989) dated through radiolarians four upper Eocene sequences from different locations (Playa Yumaque, Quebrada Perdida, Quebrada Santa Cruz and Fundo Desbarrancado).

Eocene calcareous nannofossils along the stratigraphic columns analysed in this work are dominated by large placoliths, with low diversity. Many species representing stratigraphic markers are rare (*R. erbae*, *C. grandis*, *C. oamaruensis*, *S. spiniger*, *D. saipanensis*, *D. barbadiensis*) or absent (*R. isabellae*, some

Sphenolithus species), thus preventing the full application of the high-resolution biostratigraphic scheme developed by Agnini et al. (2014) for low and middle latitudes. However, comparison among the four main sediment columns (Figure A.2, A.4) confirms the stratigraphic position of the identified bioevents and allows their correlation to build a robust age model (Figure 6).

Additional bioevents have been considered for strengthening local correlations and are related to *R. reticulata*, *Neococcolithes* and *P. multipora* (Figure 5).

R. reticulata is present with low abundance in the lower part of the sections, not only close to its first occurrence at 42.37 Ma, but even well within its range (i.e. after the first occurrence of *R. stavensis*, 40.3 Ma). It becomes common to abundant since the interval within the last occurrences of *S. spiniger* and *C. solitus*. This local event, although not biostratigraphically dated, represents a useful local correlation event that occurs close to the top of the Yumaque member.

The Top of *Neoccolithes* sp. is considered by Perch-Nielsen (1985a) as an approximation of the Bartonian-Priabonian limit. *Neococcolithes* species are rare in our samples, but their last occurrence can be traced from the RIO to the OT-Sections and occurs at the top of the Yumaque member.

Finally, *P. multipora* is rare and scattered along the sections, but becomes common close to the first occurrence of *I. recurvus* and can thus be used to locally strengthen the correlation.

The diatomaceous portion of the Otuma Formation contains typical late Eocene species. Among these *C. fennerae* (in RIO samples) indicates the *C. fennerae* biozone, also confirmed by the presence of *H. grassus* (LO at 35.1 Ma, Expedition 320/321 scientists, 2010). Accordingly, several specimens of a transitional form between *Azpeitia tuberculata* (FO 45.8 Ma, LO 34.2 Ma) and *Azpeitia oligocenica* (FO 34.2 Ma, 20.5 Ma) indicate a time span between 37.0 and 33.9 Ma (Barron et al., 2014). Similarly, a late Eocene age determination was obtained through diatom biomarkers by Fourtanier and Macharé (1988) and Macharé and Fourtanier (1988) west of the Ica River and further south along the Ica River in Fundo Desbarrancado (Figure 2). Differently, at Cerro Tiza, a few kilometres west of the Zamaca study area, DeVries et al. (2017) reported a sample (DV 591-1) containing diatom *Rouxia obesa*, which has its first occurrence in foram Zone P18 (about 33.8 to 32 Ma; see Berggren et al., 1995) suggesting an early Oligocene age for the top of the Otuma Formation at that location. The apparently contradictory age of the uppermost strata of the Otuma

Formation throughout this portion of the basin is probably due to the prominent angular unconformity at the contact with the overlaying Chilcatay Formation, which controls the exposure of Otuma sediments of different ages.

Silicoflagellates were not recorded from the deep-sea Eocene sequences off Peru (Martini, 1990b), but are reported from some sparse samples from the East Pisco Basin (Bukry, 1987). In the sections analysed here, all the silicoflagellate species support a middle-late Eocene age: *N. foliacea* spans the Eocene, with rare occurrences in the early Oligocene (McCartney et al., 2020), while *C. jerseyensis*, *C. hastata incohata* (Bukry, 1987) and *B. apiculata* (Barron et al., 2015) are restricted to the upper middle to late Eocene. *Dictyocha hexacantha* is the marker species for the *D. hexacantha* range zone (43.6-36.6 Ma, Barron et al., 2015): its co-occurrence with *B. apiculata* points to the upper part of its range and its last occurrence is probably slightly younger in our section, as the species is present well above the FO of the calcareous nannofossil *I. recurvus* (FO 36.84), unless reworked. *D. hexacantha* is absent from the topmost diatomaceous layer (OT63), where a few specimens of the late Eocene-Oligocene *C. triacantha mediana* (FO 34.7 Ma, Barron et al., 2014) were recovered.

5.2. Age model, sedimentation rates and nature of the Paracas and Otuma Formations in the East Pisco Basin

Eocene marine deposits are not abundant in the East Pisco Basin, and are scarcely represented in the record of the DSDP-ODP cores from the submerged basins of the Peruvian margin, but are more extensively exposed in the northern uplifted forearc basins, namely the Sechura and Talara basins.

The lowermost sediments of the East Pisco Basin are mostly related to continental (DeVries, 2017) or shallow marine depositional environments (DeVries, 2019) and were tentatively attributed by DeVries (2017; 2019) to the Ypresian (56.0–47.8 Ma). Such attribution was based on similarities between the upper Caballas molluscan assemblage and that described by Olsson, 1928; 1930) from the upper part of the Chacra-Salinas Group of the Talara Basin, placed in the Ypresian by Fildani et al. (2008) and Higley (2004).

The middle and upper Eocene sedimentation of Peru is characterised by marine coastal and deep-water facies, in both the East Pisco Basin and the northern Peruvian Sechura and Talara basins (Dunbar et al., 1990; Narvàez-Rodriguez and Pardo-Arguedas, 2009; Narvàez-Rodriguez and Setembrino, 2001). Both are characterised by a discontinuous sedimentation, that records major transgressions separated by important hiatuses (Marty, 1989).

In the offshore record, calcareous nannofossil biostratigraphy allowed identification of the late Eocene zone NP20 directly on top of the basement (DSDP34-321). On the lower slope, middle Eocene (NP16-17) sedimentation with shallow-water calcareous nannofossil species and shelf assemblages of benthic foraminifera is followed by a hiatus that covers the upper Eocene (ODP112-682) up to the Oligocene (ODP112-688) or lower Miocene (ODP112-683) (Martini, 1990a); this extended hiatus is known as the IQ unconformity (Von Huene et al., 1988).

In the East Pisco Basin, at the Ica River sediment succession, the marine sediments start with the Los Choros member of the Paracas Formation, with the PaE0 unconformity directly laying on top of the basement. The Los Choros member has been referred to a time interval comprised between 43.6 Ma and 42.3 Ma (Coletti et al., 2019).

The base of the Yumaque member is time-transgressive and occurs just below or just above the first occurrence of the calcareous nannofossil *R. reticulata*, dated at 42.37 Ma (Agnini et al., 2014), as observed in the section of Media Luna (Lambert et al., 2019; Lambert et al., 2017b) and across the Ica River (Coletti et al., 2019), respectively. It was dated between 42 and 39 Ma based on radiolarians at different localities both north and south of the Zamaca locality (Dunbar et al., 1990; Marty, 1989)

The age-height plot of the identified bioevents on our composite section (Figure 6) allowed calculation of sedimentation rates for the Paracas and Otuma Formations, considering different lines of correlation.

For the Yumaque member of the Otuma formation, the average sedimentation rate ranges between 24 m/My (blue line), as calculated between the first occurrence of *R. reticulata* and the first occurrence of *R. stavensis*, to 17 m/My (orange line), as calculated between the first occurrence of *R. reticulata* and the first occurrence of *R. erbae*/C*. oamaruensis*, which are very close to each other in time (37.88/37.84 Ma) and space. The last occurrence of *S. spiniger* is well constrained among sections but is a time-transgressive

event (Top common of Agnini et al., 2014, corresponding to ~40.1 Ma, but ranging from 37.32-40.40 Ma, Fornaciari et al., 2010). Similarly, the last occurrence of *C. solitus* is a diachronous event at different latitudes (39.8-38.7 Ma, Agnini et al., 2014). Both lines of correlation cross the range of *S. spiniger* LO and cross or fall close to the range of *C. solitus* LO and are therefore equally likely. Following them up to the contact with the base of the Otuma Formation, they indicate an age of ~37 to 38 Ma for the top of the Yumaque member of the Paracas Formation. It is worth to note that *R. erbae* is still present at the top of the section and its LO (37.46 Ma, Agnini et al., 2014) occurs across the Paracas-Otuma boundary. It is therefore likely to consider an average sedimentation rate of 20-21 m/My (black line) throughout the Yumaque member of the Paracas Formation, to account for this evidence.

The base of the Otuma Formation (OE0 unconformity) has been recently re-evaluated on the field in the Zamaca area (DeVries et al., 2017) and our work follows these author's definition. The FO of the calcareous nannofossil marker *I. recurvus*, calibrated at 36.84 Ma (but a spike in *I. recurvus* is calibrated at 37.46 Ma), occurs just above this base (at slightly different height among the different sections, as indicated by a large vertical bar in Figure 6). Calcareous nannofossil biostratigraphy at Media Luna (Lambert et al., 2017b; 2019) identified the first occurrence of *I. recurvus* within the Yumaque member of the Paracas Formation, probably based on the lithological identification of the Otuma Formation with the diatomite layers.

^{39}Ar-^{40}Ar dating of three tephra layers within the newly-defined Otuma Formation gave ages of 37.2 Ma (87DV509 1A-Snee) and 36.5 Ma (87DV509 1B-Snee) close to its base (see position of these layers in our Figure 2 and 4e) and 35.7 Ma (87DV508 1 Snee) further upward (DeVries, 1998). The latter date is consistent with our diatom biostratigraphic data from samples just above it (ZAMA32, 33), even though it is slightly older and the uncertainty is unkonwn. More recent dating of a tephra layer sampled just above the base of the Otuma Formation gave a sanidine-based ^{39}Ar-^{40}Ar date of 36.98 ± 0.04 Ma (AV18 in Uhen et al., 2011).

Therefore, based on previous absolute tephra dating and our nannofossil evidences, the base of the Otuma Formation can be defined at ~37 Ma. A sedimentation gap of at least 0.5 Ma is therefore likely across the Paracas-Otuma boundary, as also suggested by the transgressive nature of the basal Otuma layers.

In the Zamaca sections of the Ica River analysed here, the Otuma Formation is truncated at the top, at different heights, by the transgressive sandstones of the Chilcatay Formation (CE0 unconformity). No further bioevents are identified in the EO-Section and RIO-Section, whereas the last occurrence of *R. reticulata* (35.24 Ma, Agnini et al., 2014) was identified along the OT-Section, even though the absence of these species could be due to poor preservation of the calcareous nannofossils assemblages in these upper layers. Given that *D. saipaneneis* and *D. barbadiensis* are present up to the contact with the overlying Chilcatay Formation, the uppermost section is at least older than their LO (34.4 Ma, Agnini et al., 2014). In order to account for the possible variables, two correlation lines were considered: one that crosses the supposed LO of *R. reticulata* (orange line), resulting in a sedimentation rate of 147 m/My, the other considering that *R. reticulata* persists slightly upwards and considering the lowest height for the FO of *I. recurvus* (blue line), resulting in a sedimentation rate of 170 m/Ma. Indeed, there is a large shift in sedimentation rates at the Paracas-Otuma boundary, probably related to an increased input of terrigenous material that, as observed in smear slides, dilutes the carbonate biogenic fraction and, subsequently, to the diatom pulse.

Sedimentation rates for the Yumaque-Otuma sequence at Media Luna (Lambert et al., 2017b; 2019) range from 12 m/My in the lowermost 28 m of the Yumaque member, through 20 m/My in the interval from 40 m to 62 m, to 25 m/My in the uppermost Yumaque member, the latter roughly corresponding with the basal part of the Otuma Formation in our section.

Sedimentation rates are indeed highly variable in the East Pisco Basin and range from 160 to 320 m/My in the upper Miocene Pisco Formation (Gariboldi et al., 2017) to 160 m/My in the Quaternary of the West Pisco Basin (Suess and Von Huene, 1988). High resolution radiometric dating of sediments from the offshore deposits of Peru revealed the following sedimentation rates: 40-60 m/My in the middle-early Holocene, 30 cm/kyr at the base of the Holocene, 70-100 cm/kyr in the late Holocene and 265 cm/kyr in post-LGM early deglacial (Skilbeck and Fink, 2006).

Diatomites were only recovered at the top of the northern RIO and OT-Sections and at the ZAMA location, but were absent in the southernmost EO-Section due to the removal of the diatom-rich upper Otuma Formation at the angular erosional upper contact with the Chilcatay Formation. At the OT-Section, the

youngest nannofossil-bearing sample above the diatomite layers restrict the Otuma Formation to the zone NP19/20, as *D. saipanensis* (LO at 34.44 Ma) is still present. The absence of this species from the top samples of the northern short ZAN-Section, just below the base of the basal Chilcatay unconformity, points to the transition to zone NP21, but this evidence is not robust, as the calcareous nannofossil assemblages are strongly depleted there. Zone NP21 is indeed identified at the top of the Media Luna section (Lambert et al., 2019; Lambert et al., 2017b), but could be missing in our study area due to the erosional contact with the overlying Chilcatay Formation. As can be predicted by the northward dipping of the Otuma strata, younger Otuma layers are likely present in the subsurface further north, below the Chilcatay strata, and therefore not exposed.

Diatom and silicoflagellate species recovered from the upper diatomaceous Otuma strata support a late Eocene age, restricted to the diatom *Cestodiscus fennerae* zone and the silicoflagellate *Dictyocha hexacantha* zone and *C. apiculata* zone for the topmost sample.

It is worth to note that the LO of *D. hexacantha* is probably slightly younger here than indicated in previous work (Barron et al., 2014, 1015), as compared to calcareous nannofossil and diatom biozones (see Figure 3).

Late Eocene diatomaceous sediments are documented at other locations in the East Pisco Basin, from Fundo Desbarrancado (referred to as sediments of the upper Yumaque, Dunbar et al., 1990; Fourtanier and Macharé, 1988; Marty et al., 1988), Salinas de Otuma and west of Ica River (Fourtanier and Macharé, 1988) and their diatom content confirms a late Eocene age. For the upper Eocene laminated diatomites at Fundo Desbarrancado, Marty et al. (1988) and Marty (1989) calculated a sedimentation rate of 780 m/My from the study of annual varves and these values are close to those calculated for the Miocene diatomites in the Sechura Basin (Marty et al., 1998). Such data cannot however be compared with our analysis, which considers average sedimentation rates for the whole Otuma Formation.

At Quebrada Perdida, DeVries et al. (2017) identified a glauconite-rich layer on top of the diatomites and attributed it to the Eocene-Oligocene transition (EOT), based on sparse age assignments of the uppermost layers of the Otuma Formation (DeVries et al., 2006). Such layer however has not been encountered along our sections at Zamaca nor across the Ica River area, likely because the latter sections are truncated below this event (or because the event is laterally discontinuous).

A glauconite layer is reported by DeVries et al. (2017) a few km west of Zamaca at Cerro Tiza, corresponding to the location of a single diatom-based early Oligocene age for the Otuma sediments. However, only a complete section measured at Cerro Tiza with accurate sampling for bio- and tephrotratigraphic dating will allow to define if and how the EOT is preserved in this area.

5.3. Paleoclimatic and paleoceanographic trends

The middle-upper Eocene sequence of the East Pisco Basin provides a long, albeit discontinuous, record of paleoceanographic variations occurring along the Peruvian shelf, in a time interval characterised by significant climatic variations (Zachos et al., 2008; Zachos et al., 2001; Westerhold et al., 2000). An overall cooling trend occurs from the early Eocene climatic optimum to the onset of the Icehouse conditions at the base of the Oligocene, involving significant oceanographic changes at the EOT. This cooling phase is interrupted by several small-scale fluctuations (Figure 3), among which are the Late Lutetian Thermal Maximum and the Middle Eocene Climatic Optimum (MECO), a transient ~500 kyr interval of 4–6°C warming, starting around 41.5-40.45 Ma, which was followed by a rapid throwback to the pre-existing thermal regime (Bohaty and Zachos, 2003; Bohaty et al., 2009; Westerhold and Röhl, 2013; Westerhold et al., 2020).

In our study area, the benthic fauna of the Los Choros member of the Paracas Formation (upper Lutetian) testifies to a tropical setting, suitable for abundant large benthic foraminifera, including the extant tropical genus *Amphistegina* (Coletti et al., 2019; Morales-Reyna et al., 2010; Morales-Reyna et al., 2013), with moderate nutrient supply providing sustenance for barnacles.

The Yumaque member of the Paracas Formation (upper Lutetian – lower Priabonian) is peculiar for its continuous record of calcareous nannofossils that are otherwise not present or scattered and poorly preserved in the younger formations of the East Pisco Basin. This suggests that carbonate production or preservation was higher in the middle-early late Eocene and then decreased towards the Oligocene and upwards. Such a trend contrasts with the open-ocean record of the subtropical and equatorial Pacific, which recorded a sudden increase in calcite dissolution around the MECO (Toffanin et al., 2013) and a

sudden drop in the calcite saturation depth at the EOT (Coxall et al., 2005; Pälike et al., 2012; Rea and Lyle, 2005), resulting from a reorganization of the global ocean linked to sudden cooling as well as to the onset of the Antarctic glaciation. Such contrast in carbonate production/preservation can be interpreted as due to peculiar local conditions, that differ from the more general picture of the subtropical and equatorial Pacific.

Calcareous nannofossils across the late Eocene have been studied by several authors at different locations and seem to correlate with changes in both temperature and nutrient supply. In particular:

- *Sphenolithus* spp., *C. formosus*, *Discoaster* spp. are identified as warm and oligotrophic taxa (Aubry, 1992; Bralower, 2002; Gibbs et al., 2006; Villa et al., 2008; Wei et al., 1992; Wei and Wise, 1990);
- *R. bisecta* is considered a temperate/warm species (Persico and Villa, 2004; Wei et al., 1992) that evolved close to the MECO;
- *C. pelagicus* and *C. eopelagicus* are considered temperate species (Villa et al., 2014)
- *R. reticulata* is generally regarded as an oligotrophic taxon that is more abundant at high latitudes than at low latitudes (Wei et al., 1992; Wei and Wise, 1990); consequently, it is generally indicated as a cool species at temperate/cold latitudes (Villa et al., 2008) or as a temperate species at cold latitudes (Villa et al., 2014).
- *R. daviesii*, *I. recurvus* and *Chiasmolithus* spp. are generally regarded as typical of cool waters (Monechi et al., 2000; Villa et al., 2008; Wei et al., 1992). As for their trophic preference, *I. recurvus* shows a preference for eutrophic waters (Villa et al., 2014), while *Chiasmolithus* spp. are considered as mesotrophic (Aubry, 1998; Bralower, 2002; Kalb and Bralower, 2012) or oligotrophic (Gibbs et al., 2006)
- *Helicosphaera* is considered a mesotrophic to eutrophic genus (De Kaenel and Villa, 1996; Guerreiro et al., 2005; Ziveri et al., 2004).

Analyses of calcareous nannofossili trends typically indicate an increase of cold (Villa et al., 2008; Wei et al., 1992) and eutrophic (Fioroni et al., 2015) taxa towards the EOT, indicating an overall cooling and a reorganization of water masses.

In the Yumaque/Otuma sediments, the calcareous nannofossil assemblage is often depleted, and the analyses were only carried out semi-quantitatively, however some trends can be detected, mainly by looking at the pattern of placoliths.

The basal Yumaque sediments (42.38 - ~38 Ma) reflect warm-temperate conditions, as testified by low abundances of the cool water *R. reticulata*, the frequent abundance of the temperate *R. bisecta* (since its first occurrence), the presence of *C. pelagicus-C. eopelagicus* as well as of the warm-oligotrophic *C. formosus*. The warm water *Sphenolithus* spp. and *Discoaster* spp., are present with low abundance, as well as the cool *Chiasmolithus* spp. The other cold-water species, *R. daviesii*, is scattered throughout the sections and does not allow for detecting an abundance trend.

While cool water conditions were inferred for the Yumaque by Uhen et al. (2011), the small benthic foraminifera and calcareous nannofossil species indicated therein are in fact not restricted to cold waters (Coletti et al., 2019). Rather, the presence of the shallow-water nectobenthic genus *Pristis* (Collareta et al., 2020b), known as a tropical/subtropical fish, supports the calcareous nannofossil evidence of warm-temperate conditions.

In the upper Yumaque, since ~38 Ma, *R. reticulata* shows a significant increase, paralleled by a slight decrease in the warm-water *C. formosus* and in the temperate *D. bisecta*, *C. eopelagicus* and *C. pelagicus*, likely reflecting a cooling trend. Both warm and cold water non-placolith taxa dramatically decrease in abundance in the overlying sediments, but this probably represents an artifact induced by the poor preservation state of this assemblage. *I. recurvus* appears just above the base of the Otuma Formation and confirms the presence of cool conditions throughout the interval of deposition, as this species is typically lacking in low latitudes.

Species indicative of coastal conditions (*Z. bijugatus*, *Pemma* spp., *Micrantholithus* spp.) are present in the basal and top intervals of the Yumaque member as well as at the base of the Otuma Formation.

Regarding the trophic conditions, in the lower part of the Yumaque there is contrasting evidence coming from the oligotrophic *Sphenolithus* spp. and *Discoasters* spp. on the one hand and the eutrophic *Chiasmolithus* spp. on the other hand. *Helicosphaera* species become more abundant between ~40 and ~37 Ma, thus testifying to increasing nutrient contents in this interval spanning the top of the Paracas and the basal Otuma layers.

Abundant small-sized fish scales occur throughout the Yumaque-Otuma succession and have been attributed to clupeoid fish (Uhen et al., 2011) and thus used as an indication of upwelling conditions.

However, such scales cannot be positively identified as belonging to any member of Clupeoidea (Collareta et al., 2020b) and thus cannot be used as an unambiguous indication of upwelling.

The presence of diatomites at the top of the Otuma Formation has also been considered as a proxy for upwelling conditions (Marty et al., 1988; Marty, 1989), leading to the inference of a late Eocene development of a proto-Humboldt current associated with significant cooling. Late Eocene (37.5-33.5 Ma) diatomites from the sub-Antarctic South Atlantic (Diekmann et al., 2004; Barron et al., 2014) were indeed attributed to upwelling, related to a reorganization in ocean circulation occurring at that time in the Southern Ocean. Late Eocene-Oligocene increased abundance of species richness and diversity of *Chaetoceros* resting spores were also detected in the north-Atlantic (Suto et al., 2012) and attributed to the initiation of upwelling.

However, examination of the diatom species occurring in the upper Otuma layers indicates not only the presence of high productivity genera, like *Chaetoceros* and rarer *Thalassionema*, but also the abundance of genera such as *Hemiaulus*, *Pyxilla*, *Rhizosolenia*, *Stephanopyxis* and large *Coscinodiscus* and *Cestodiscus* that are typical of a deep-chlorophyll maximum and/or can develop a symbiosis with nitrogen-fixers (Kemp, et al., 2000). Such genera are indicative of production deep in the water column in environments characterised by increased spring nutrient supply and nutrient-depleted stratified summer waters, with summer primary production carried out by these large species, responsible of the “fall dump” (Kemp et al., 2000). As also demonstrated using a species-based approach on other diatom-rich sediments (Davies and Kemp, 2016), upwelling was seasonally-limited in the upper Otuma times in this portion of the East Pisco Basin. The large and robust taxa *Hemiaulus*, *Stephanopyxis*, and *Pyxilla* are typical of the late Eocene floras, that decline during the early Oligocene (Barron and Baldauf, 1995), probably outcompeted by smaller and less silicified species. The common presence of the neritic diatom genus *Paralia* (Witkowski et al., 2014) and the presence of the benthic genus *Actinoptychus* indicate proximity to the coast.

Climatic evidence from radiolarian assemblages indicate warm water conditions for these late Eocene intervals (Fourtanier and Macharé, 1988). No cold-water diatoms were recovered. Silicoflagellates recovered in the diatomites, although rare, are mainly represented by the temperate-warm water genera *Corbisema* and *Naviculopsis*, with *Corbisema* > *Naviculopsis*, an index for warm conditions (i.e. Bukry,

1987). *D. hexacantha*, used in the low-latitude zonation (Perch-Nielsen, 1985b), was recovered from a few samples, while the genus *Stephanocha*, typical of cold conditions, is notably absent. Only a few specimens of *S. speculum* and *D. crux* were recovered from the topmost sample of the OT section.

Overall, the Otuma strata record temperate climatic conditions, with a slight cooling trend upwards and an increase in nutrient availability, indicated by the shift from calcareous to siliceous sedimentation. These lines of evidence suggest the onset, during the late Otuma times, of a slight upwelling, which can be correlated with the significant reorganization of the circum-Antarctic circulation and the beginning of a proto-Humboldt current. However, upwelling was seasonally limited, with persisting summer stratified and nutrient-depleted conditions, dissimilar from the full-upwelling conditions that took place in the Miocene as documented from the Pisco Formation (e.g. Gariboldi et al., 2017).

6. Conclusions

Biostratigraphic analyses carried out along four main stratigraphic sections from the Paracas and Otuma formations exposed in the area of Zamaca astride the Ica River allowed the definition of a biostratigraphic framework for this important middle-upper Eocene Fossil Lagerstätte.

The Yumaque member represents the fine-grained upper portion of the Paracas Formation, grading from the coarser Los Choros member. Its base falls around the first occurrence of *R. reticulata* (42.37 Ma) and its top occurs just above the FO of *R. erbae / C. oamaruensis* (37.88/37.84 Ma) and before the LO of *R. erbae* (37.46 Ma). Sedimentation rates within the Yumaque member fall within the range of 17-24 m/My. The Yumaque strata witness overall temperate-warm conditions, with a moderate to good degree of preservation of calcareous nannofossils and a cooling trend detected since ~38 Ma, linked to the global cooling and/or the development of a weak upwelling. Mesotrophic conditions are present for most part of the Yumaque, excluding the basal layers.

The base of the Otuma Formation occurs just below the first occurrence of *I. recurvus* (36.84 Ma, but this species has a spike at 37.46 Ma) which gives an age that is consistent with previous radiometric dating at 37.2 Ma, 36.5 Ma and 36.98 ± 0.04 Ma. The Otuma Formation has been reported to be early Oligocene at

other locations of the East Pisco Basin. However, in the studied sections of the Ica River Valley, its upper diatomaceous part is restricted to the late Eocene *Cestodiscus fennerae* zone, with age constrains given by the LO of *R. reticulata* (35.2 Ma), the LO of *H. grassus* (35.1 Ma), the LO of *C. fennerae* (34.1 Ma), the FO of *C. triacantha mediana* (34.7 Ma) and the LO of *D. saipaneneis* (34.4 Ma). Therefore, the upper range of the marker species *D. hexacantha* (LO 36.6 Ma) should be extended at least locally.

Average sedimentation rates in the Otuma Formation, calculated between the FO of *I. recurvus* and the LO of *R. reticulata* at the OT section, range from 147 to 170 m /My, much higher than the Yumaque member of the Paracas Formation, probably due to increasing accumulation of terrigenous material and diatomites. Calcareous nannofossils indicate an overall cooling trend for the Otuma Formation as compared to the Yumaque member, but silicoflagellate genera are still indicative of temperate conditions and diatoms species still belong to the temperate settings. Diatomites at the top of the Otuma Formation represent a shift from calcareous to siliceous productivity testifying to an overall increase in nutrients, but diatom genera are adapted to exploit a deep nutrient supply in stratified water, consistent with a seasonally-limited rather than a sustained year-round upwelling.

Figure captions

Figure 1. a) Map of the sedimentary basins of the Peruvian margin, with DSDP-ODP sites b) sediment fill of the East Pisco Basin (modified after DeVries, 1998). The intervals studied in this work are indicated in colour.

Figure 2. Unpublished geologic map of the study area based on 1:10,000 mapping. This figure shows the position of the four measured sections in Fig. 4a to 4i used to construct the correlation panel in Fig. 5 and the location of the ZAN and ZAMA localities. The stars represent locations of previous studies of Eocene deposits. The inset displays the location map of the study area along the Ica River and the position of the localities mentioned in the text, namely Salinas de Otuma (SdO); Playa Yumaque (PY); Quebrada Perdida

(QP); Media Luna (ML); Cerro Tiza (CT); Fundo Desbarrancado (FD); Quebrada Santa Cruz (QSC); Quebrada Huaricangana (QH).

Figure 3. Biostratigraphic zonal schemes and relative bioevents for the Middle Eocene - Early Oligocene time frame of the Paracas and Otuma Formation and climatic framework. Calcareous nannofossils zones CN (Agnini et al., 2014), NP (Martini, 1971), CP (Okada and Bukry, 1980) and diatom zones (Barron et al., 2015) were plotted with Time Scale Creator using the GPTS2020 of Gradstein et al. (2020) and redrawn in Corel Draw; silicoflagellate zones are correlated to diatoms zones from Barron et al., (2015); the benthic oxygen isotope curve is from Westerhold et al. (2020).

Figure 4. Panoramic photos of the measured outcrops. a, EO-Section (base: 14°42'21.3"S - 75°35'9.9"W; top: 14°42'7.1"S - 75°35'9.6"W). Encircled persons for scale; b, RIO-Section (base: 14°41'21.60"S - 75°36'43.20"O; top: 14°41'16.0"S - 75°36'23.0"W). Scale bar = 50 m; c, MB-Section (base: 14°40'54.4"S - 75°37'42.9"W; top: 14°40'45.8"S - 75°37'46.3"W). Encircled person for scale; d, OT-Section (base: 14°39'54.5"S - 75°38'11.0"W; top: 14°39'21"S - 75°38'31.9"W). Scale bar = 50 m; e, panoramic view of the Paracas-Otuma unconformity (14°39'42"S - 75°37'56"W), with the two ash layers in the basal Otuma Formation. Scale bar = 50 m; f, close up of the boulder layer at the OE0 unconformity. Scale bar = 1 m; g, detail of the central portion of the OT-Section showing position of photos in h and i. The two continuous black lines indicate position of two marker beds and their heights in meters above the base of the section. Scale bar = 10 m; h, close up of the finely laminated silts forming the bulk sediments of the Otuma Formation. Hammer for scale; I, close up of the three thin tephra layers intercalated in the diatomaceous portion in the upper portion of the Otuma Formation. Hammer for scale.

Figure 5. Correlation panel of the measured stratigraphic sections and location of the identified bioevents.

Figure 6. Age model for the upper Paracas-Otuma sequence, based on calcareous nannofossili events, as calibrated in Agnini et al. (2014). The vertical axis is in EO-section meters abs for all vertical sections (see 3.3 and Figure A.3). ONE COLUMN

Figure 7. Main calcareous nannofossil species from the Paracas and Otuma formations: 1) *C. eopelagicus* (MB18); 2) *R. umbilicus* (MB17); 3) *R.dictyoda* (RIO-D9), 4) *C. formosus* (MB18); 5) *R.bisecta* (MB17); 6) *R. stavensis* (EO-D26); 7) *R. reticulata* (MB23); 8) *R. lockerii* (RIO-D15); 9) *C. floridanus* (EO-D65); 10) *C. grandis* (MB15); 11) *C. solitus* (MB18); 12) *C. titus* (MB21); 13) *H. reticulata* (MB25); 14) *H. clarissima* (MB18); 15) *H. compacta* (MB18); 16) *H. wilcoxonii* (OT23); 17) *P. multipora* (RIO-D23); 18) *P. exilis* (RIO-D15); 19) *P. obliquipons* (RIO-D15); 20) *N. minutus* (MB17); 21) *I. recurvus* (RIO-D23); 22) *S. spiniger* 0° and 45° (MB18); 23) *S. radians* (MB18); 24) *S. furcatulithoides* (MB23); 25) *Z. bijugatus* (MB23); 26) *P. basquense* (MB25); 27) *P. papillata* (MB25); 28) *Micrantholithus* sp. (RIO-D15); 29) *D. saipanensis* (RIO-D11); 30) *D. nodifer* (MB18); 31) *B. spinosus* (MB18); 32) *C. dela* (MB17). Scale bar = 10 μm for all images.

Figure 8. Main diatom (1-22, 27), silicoflagellate (23-26), ebridian (28) and incertae saedis (29) species from the Paracas and Otuma formations: 1) *P. gracilis* (OT47); 2, 3) *P. reticulata* (OT45); 4) *P. reticulata* (*P. johnsoniana* Forti) (OT38); 5) *P. reticulata* (*P. johnsoniana* var. *corniculum*), low and high focus (OT45); 6) *P. johnsoniana* Greville, low and high focus (RIO-D39); 7) *H. polymorphus* var. *morsianus*, low and high focus (ZAMA33): the arrow indicates the broader and higher central segment; 8) *H. grassus*, low and high focus (OT63): the arrow indicates the central segment, similar in height and width to the other segments; 9) *Cestodiscus pulchellus var. novazealandica* (RIO-D40); 10) *Cestodiscus fennerae* low and high focus (RIO-D40); 11, 12) *H. altus* (RIO-D36); 13, 14) *H. subacutus* (RIO-D41, RIO-D36); 15) *H. subacutus* with basal constrictions (OT63); 16, 17) *H. polycystinorum* (OT39, OT63); 18) *H. grassus* (OT63); 19) *A. splendens* (OT47); 20) *Cestodiscus* aff. *intersectus* (OT45); 21, 22) *Azpeitia tuberculata-oligocenica* low and high focus (ZAMA325); 22) *D. architecturalis* (OT63); 23) *B. apiculata* (ZAMA32); 24) *N. foliacea* (ZAMA32); 25) *D. hexacantha* (OT47); 26) *C. triacantha* s.l. (ZAMA32); 27) *P. aculeifera* (ZAMA32); 28) *M. barbadense* (OT63); 29) *E. crenulata* (ZAMA32). Scale bar = 10 μm for all images.

Supplementary material: captions

Figure A.1: Table of species occurrences along the measured sections.

Figure A.2: List of calcareous nannofossil bioevent height identified along the different sections and height data for the correlation of the different sections.

Figure A.3: Stratigraphic ranges of biostratigraphically-useful species.

Figure A.4: Age models calculated for each stratigraphic section.

Acknowledgments

We would like to thank John Barron for precious suggestions on diatom taxonomy and in particular on the identification of *Cestodiscus* species and Thomas J. DeVries for fruitful discussions on the stratigraphy of the Otuma Formation and the Pisco Basin geology. Our gratitude to Olivier Lambert, Rafael M. Varas-Malca, Walter Aguirre, for their support in the field, as well as for much useful discussions on the geology and paleontology of the Pisco Basin and to Giovanni Coletti for useful discussion on biostratigraphy. We also wish to thank two anonymous reviewers for useful comments that significantly improved the discussion of the paper.

CRediT author statement

Elisa Malinverno: Conceptualization; Field work and photos; Data curation; Formal analysis; Validation; Funding acquisition; Investigation; Methodology; Writing - original draft and editing; Visualization.

Giulia Bosio: Field work and photos; Formal analysis; Validation; Investigation; writing – review and editing; Visualization.

Claudio Di Celma: Field work and photos; Funding acquisition; Investigation; Methodology; Software; Writing – review and editing; Visualization

Karen Gariboldi: Field work; Validation; Investigation; Writing – review and editing

Anna Gioncada: Field work; Writing – review and editing

Pietro Paolo Pierantoni: Field work; Writing – review and editing

Alberto Collareta: Field work; Writing – review and editing

Giancarlo Molli: Field work; Writing – review and editing

Gabriella Bagnoli: Field work; Writing – review and editing

Giovanni Sarti: Field work; Writing – review and editing

Mario Urbina: Field work

Giovanni Bianucci: Field work, Funding acquisition; Project administration; Writing – review and editing.

Funding

Fieldwork was supported by grants from the Italian Ministero dell'Istruzione, dell'Università e della Ricerca (MIUR) to Bianucci (PRIN Project, 2012YJSBMK EAR- 9317031), Malinverno (PRIN Project, 2012YJSBMK_002), Di Celma (PRIN Project, 2012YJSBMK 003); the University of Camerino (FAR 2019 grant); the University of Pisa to Bianucci (PRA_2017_0032).

References

Agnini C, Fornaciari E, Raffi I, Catanzariti R, Pälike H, Backman J, Rio D (2014) Biozonation and biochronology of Paleogene calcareous nannofossils from low and middle latitudes. Newsletters on Stratigraphy 47: 131-181

Arney JE, McGonigal KL, Ladner BC, Wise SW, Jr. (2003) Lower Oligocene to Middle Miocene diatom biostratigraphy of ODP site 1140, Kerguelen Plateau. In: Frey FA, Coffin MF, Wallace PJ, Quilty PG (eds) Proceedings of the Ocean Drilling Program, Scientific Results, pp 1-21

Aubry MP (1992) Late Paleogene calcareous nannoplankton evolution: a tale of climatic deterioration. In: Prothero DR, Berggren WA (eds) Eocene-Oligocene Climatic and Biotic Evolution. Princeton University Press., Princeton, NJ, pp 272-309

Aubry MP (1998) Early Paleogene calcareous nannoplankton evolution: a tale of climatic amelioration. In: Lucas MP, Berggren WA (eds) Late Paleocene-Early Eocene Climatic and Biotic Events int he Marine and Terrestrial Records. Columbia University Press, New York, pp 158-203

Balarezo VEPR, Samame BM, Morales AB (1980) Sinopsis explicativa del mapa del Departamento de Ica. Inst. Geol. Miner. Metal. Lima, Bol. Ser. F 2: 27 pp

Barron J (1985) Miocene to Holocene Planktic diatoms. In: Bolli HM, Saunders JB, Perch-Nielsen K (eds) Plankton Stratigraphy. Cambridge, pp 763-810

Barron J, Bukry D, Gersonde R (2014) Diatom and silicofllagellate biostratigraphy for the late Eocene: ODP 1090 (sub-Antarctic Atlantic). Nova Hedwigia, Beihefte 143: 1-31

Barron J, Bukry D, Poore RZ (1984) Correlation of the middle Eocene Kellogg Shale of northern California. Micropaleontology 30: 138-170

Barron J, Stickley CE, Bukry D (2015) Paleoceanographic, and paleoclimatic constraints on the global Eocene diatom and silicoflagellate record. Palaeogeography, Palaeoclimatology, Palaeoecology 422: 85-100

Barron JA, Baldauf JG (1995) Cenozoic marine diatom biostratigraphy and applications to paleoclimatology and paleoceanography. Paleontological Society Short Courses in Paleontology 8: 107-118

Bianucci G, Collareta A, Bosio G, Landini W, Gariboldi K, Gioncada A, Lambert O, Malinverno E, de Muizon C, Varas-Malca RM, Villa IM, Coletti G, Urbina M, Di Celma C (2018) Taphonomy and palaeoecology of the lower Miocene marine vertebrate assemblage of Ullujaya (Chilcatay Formation, East Pisco Basin, southern Peru). Palaeogeography, Palaeoclimatology, Palaeoecology 511: 256-279

Bianucci G, De Muizon C, Urbina M, Lambert O (2020) Extensive diversity and disparity of the early Miocene platanistoids (Cetacea, Odontoceti) in the southeastern Pacific (Chilcatay Formation, Peru). Life 10

Bianucci G, Di Celma C, Collareta A, Landini W, Post K, Tinelli C, de Muizon C, Bosio G, Gariboldi K, Gioncada A, Malinverno E, Cantalamessa G, Altamirano-Sierra A, Salas-Sigismondi R, Urbina M, Lambert O (2016a) Fossil marine vertebrates of Cerro Los Quesos: Distribution of cetaceans, seals, crocodiles, seabirds, sharks, and bony fish in a late Miocene locality of the Pisco Basin, Peru. Journal of Maps 12: 1037-1046

Bianucci G, Di Celma C, Landini W, Post K, Tinelli C, de Muizon C, Gariboldi K, Malinverno E, Cantalamessa G, Gioncada A, Collareta A, Salas-Sigismondi R, Varas-Malca RM, Urbina M, Lambert O (2016b) Distribution of fossil marine vertebrates in Cerro Colorado, the type locality of the giant raptorial sperm whale *Livyatan melvillei* (Miocene, Pisco Formation, Peru). Journal of Maps 12: 543-557

Bianucci G, Di Celma C, Urbina M, Lambert O (2016c) New beaked whales from the late Miocene of Peru and evidence for convergent evolution in stem and crown Ziphiidae (Cetacea, Odontoceti). PeerJ 4: e2479

Blechschmidt G (1976) Biostratigraphy of calcareous nannofossils: Leg 34, Deep Sea Drilling Project Initial Reports of Deep Sea Drilling Project, pp 705-712

Bohaty S, Zachos JC (2003) Significant Southern Ocean warming event in the late middle Eocene. Geology 31: 1017-1020

Bohaty S, Zachos JC, Florindo F, Delaney M (2009) Coupled greenhouse warming and deep-sea acidification in the Middle Eocene. Paleoceanography 24: PA2207

Bosio G, Gioncada A, Malinverno E, Di Celma C, Villa IM, Cataldi G, Gariboldi K, Collareta A, Urbina M, Bianucci G (2018) Chemical and petrographic fingerprinting of volcanic ashes as a tool for high-resolution stratigraphy of the upper Miocene Pisco Formation (Peru). Journal of the Geological Society

Bosio G, Malinverno E, Collareta A, Di Celma C, Gioncada A, Parente M, Berra F, Marx F, Vertino A, Urbina M, Bianucci G (2020a) Strontium Isotope Stratigraphy and the thermophilic fossil fauna from the middle Miocene of the East Pisco Basin (Peru). Journal of South American Earth Sciences 97: 102399

Bosio G, Malinverno E, Villa IM, Di Celma C, Gariboldi K, Gioncada A, Barberini V, Urbina M, Bianucci G (2020b) Tephrochronology and chronostratigraphy of the Miocene Chilcatay and Pisco formations (East Pisco Basin, Peru). Newsletters on Stratigraphy 53: 213-247

Bralower TJ (2002) Evidence of surface water oligotrophy during the Paleocene–Eocene thermal maximum: nannofossil assemblage data from OceanDrilling ProgramSite 690,Maud Rise,Weddel Sea. Paleoceanography 17: 13.11-13.13

Bukry D (1978). Cenozoic coccolith and silicoflagellate stratigraphy, offshore northwest Africa, Deep Sea Drilling Project Leg 41. In: Lancelot, Y., Seibold, E., et al., Init. Repts. DSDP, 41: Washington (U.S. Govt. Printing Office), 689-707.Bukry D (1981) Synthesis of silicoflagellate stratigraphy for Maastrichtian to Quaternary marine sedimen. SEPM Special Publication 32: 433-444

Bukry D (1987) Eocene siliceous and calcareous phytoplankton, Deep Sea Drilling Project Leg 95. In: Turner KL (ed) Initial Reports of Deep Sea Drilling Project. U.S. Government Printing Office, pp 395-415

Cervato C, Burkle L (2003) Pattern of first and last appearance in diatoms: Oceanic circulation and the position of polar fronts during the Cenozoic. Clarke JA, Ksepka DT, Salas-Sigismondi R, Altamirano-Sierra A, D'Alba M, Vinther J, DeVries TJ, Baby P (2010) Fossil evidence for evolution of the shape and color of penguin feathers. Science 330: 954-957

Clarke JA, Ksepka DT, Stucchi M, Urbina M, Giannini N, Bertelli S, Narvàez Y, Boyd CA (2007) Paleogene equatorial penguins challenge the proposed relationship between biogeography, diversity, and Cenozoic climate change. Proceedings of the National Academy of Sciences 104

Clift, P.D., Pecher, I., Kukowski, N. and Hampel, A., 2003. Tectonic erosion of the Peruvian forearc, Lima Basin, by subduction and Nazca ridge collision: Tectonic erosion of the Peruvian forearc. Tectonics, 22: 1023.

Coletti G, Bosio G, Collareta A, Malinverno E, Bracchi VA, Di Celma C, Basso D, Stainbank S (2019) Biostratigraphic, evolutionary, and paleoenvironmental significance of the southernmost lepidocyclinids of the Pacific coast of South America (East Pisco Basin, southern Peru). Journal of South American Earth Sciences 96: 102372

Collareta A, Lambert O, de Muizon C, Benites-Palomino AM, Urbina M, Bianucci G (2020a) A new physeteroid from the late Miocene of Peru expands the diversity of extinct dwarf and pygmy sperm whales (Cetacea: Odontoceti: Kogiidae). Comptes Rendus Palevol 95: 79-100

Collareta A, Landini W, Chacaltana-Budiel C, Valdivia-Vera W, Altamirano-Sierra A, Urbina-Schmitt M, Bianucci G (2017) A well preserved skeleton of the fossil shark Cosmopolitodus hastalis from the late Miocene of Peru, featuring fish remains as fossilized stomach contents. Rivista Italiana di Paleontologia e Stratigrafia 123: 11-22

Collareta A, Landini W, Lambert O, Post K, Tinelli C, Di Celma C, Panetta D, Tripodi M, Salvadori PA, Caramella D, Marchi D, Urbina-Schmitt M, Bianucci G (2015) Piscivory in a Miocene Cetotheriidae of Peru: first record of fossilized stomach content for an extinct baleen-bearing whale. The Science of Nature (Naturwissenschaften) 102: article #70

Collareta A, Tejada-Medina L, Chacaltana-Budiel C, Landini W, Altamirano-Sierra A, Urbina-Schmitt M, Bianucci G (2020b) A rhinopristiform sawfish (genus Pristis) from the middle Eocene (Lutetian) of southern Peru and its regional implications. Carnets Geol. 20: 91-105

Coxall HK, Wilson PA, Pälike H, Lear CH, Backman J (2005) Rapid stepwise onset of Antarctic glaciation and deep calcite compensation in the Pacific ocean. Nature 433: 53-57

Danelian T, Saint Martin S, Blanc-Valleron M-M (2007) Middle Eocene radiolarian and diatom accumulation in the equatorial Atlantic (Demerara Rise, ODP Leg 207) Possible links with climatic and palaeoceanographic changes. Comptes Rendus Palevol 6: 103-114

Davies A, Kemp AES (2016) Late Cretaceous seasonal palaeoclimatology and diatom palaeoecology from laminated sediments. Cretaceous Research 65: 82-111

De Kaenel E, Villa G (1996) Oligocene/Miocene calcareous nannofossil biostratigraphy and paleoecology from the Iberia Abyssal Plain, Northeastern Atlantic. . In: Whitmarsh RB, Sawyer DS, Klaus A, Masson DG (eds) Proceedings of ODP Scientific Results 149, pp 79–145

de Muizon C, Bianucci G, Martinez-Caceres M, Lambert O (2019) *Mystacodon selenensis*, the earliest known toothed mysticete (Cetacea, Mammalia) from the late Eocene of Peru: anatomy, phylogeny, and feeding adaptations. Geodiversitas 41: 401-499

DeVries TJ (1998) Oligocene deposition and Cenozoic sequence boundaries in the Pisco basin (Peru). Journal of South American Earth Sciences 3: 217-231

DeVries TJ (2017) Eocene Stratigraphy and Depositional History near Puerto Caballas (East Pisco Basin, Peru). Boletín de la Sociedad Geológica del Perú 112: 39-52

DeVries TJ (2019) Early Paleogene brackish-water molluscs from the Caballas Formation of the East Pisco Basin (Southern Peru). Journal of Natural History 53: 25-26

DeVries TJ, Narvaez Y, Sanfilippo A, Malumian N, Tapia P (2006) New microfossil evidence for a late Eocene age of the Otuma formation (Southern Peru) XIII Congreso Peruano de Geología, Lima, Peru, October, 2006. Sociedad Geológica del Perú, Publicación Especial, pp 615-618

DeVries TJ, Urbina M, Judd NA (2017) The Eocene-Oligocene Otuma Depositional Sequence (East Pisco Basin, Peru): Paleogeographic and Paleoceanographic Implications of New Data. Boletín de la Sociedad Geológica del Perú 112: 14-38

Di Celma C, Malinverno E, Bosio G, Collareta A, Gariboldi K, Gioncada A, Molli G, Basso D, Varas-Malca RM, Pierantoni PP, Villa G, Lambert O, Landini W, Sarti G, Cantalamessa G, Urbina M, Bianucci G (2017) Sequence stratigraphy and paleontology of the upper Miocene Pisco formation along the Western side of the Lower Ica Valley (Ica desert, Peru). Rivista Italiana di Paleontologia e Stratigrafia 123: 255-273

Di Celma C, Malinverno E, Bosio G, Gariboldi K, Collareta A, Gioncada A, Landini W, Pierantoni PP, Bianucci G (2018a) Intraformational unconformities as a record of late Miocene eustatic falls of sea level in the Pisco Formation (southern Peru). Journal of Maps 14: 607-619

Di Celma C, Malinverno E, Cantalamessa G, Gioncada A, Bosio G, Villa IM, Gariboldi K, Rustichelli A, Pierantoni PP, Landini W, Tinelli C, Collareta A, Bianucci G (2016a) Stratigraphic framework of the late Miocene Pisco Formation at Cerro Los Quesos (Ica Desert, Peru). Journal of Maps 12: 1020-1028

Di Celma C, Malinverno E, Collareta A, Bosio G, Gariboldi K, Lambert O, Landini W, Pierantoni PP, Gioncada A, Villa G, Coletti G, de Muizon C, Urbina M, Bianucci G (2018b) Facies analysis, stratigraphy and

marine vertebrate assemblage of the lower Miocene Chilcatay Formation at Ullujaya (Pisco basin, Peru). Journal of Maps 14: 257-268

Di Celma C, Malinverno E, Gariboldi K, Gioncada A, Rustichelli A, Pierantoni PP, Landini W, Bosio G, Tinelli C, Bianucci G (2016b) Stratigraphic framework of the late Miocene to Pliocene Pisco Formation at Cerro Colorado (Ica Desert, Peru). Journal of Maps 13: 515-529

Di Celma C, Pierantoni PP, Malinverno E, Collareta A, Lambert O, Landini W, Bosio G, Gariboldi K, Gioncada A, de Muizon C, Molli G, Marx FG, Varas-Malca RM, Urbina M, Bianucci G (2019) Allostratigraphy and paleontology of the lower Miocene Chilcatay Formation in the Zamaca area, East Pisco basin, southern Peru. Journal of Maps 15: 393-405

Diekman B, Kuhn G, Gersonde R, Mackensen A (2004) Middle Eocene to early Miocene environmental changes in the Sub-Antarctic Southern Ocean: evidence from biogenic and terrigenous depositional patterns at ODP Site 1990. Global and Planetary Change 40: 295-313.

Dunbar R, Marty RC, Baker P (1990) Cenozoic marine sedimentation in the Sechura and Pisco Basin, Peru. Palaeogeography, Palaeoclimatology, Palaeoecology 77: 235-261

Expedition 320/321 Scientists (2010) Methods. In: Pälike H, Lyle M, Nishi H, Raffi I, Gamage K, Klaus A, Scientists E (eds) Proc. IODP, 320-321. Tokyo (Integrated Ocean Drilling Program Management International, Inc.)

Fenner J (1976) Diatom phytoplankton studies in the southern Pacific Ocean. Composition, correlation to the Antarctic Convergence and its paleoecological significance. In: Hollister CD, Craddock C, al. e (eds) Initial Reports of the Deep Sea Drilling Project. U.S. Government printing office, Washington, pp 757-814

Fenner J (1984) Eocene-Oligocene planktic diatom stratigraphy in the low latitudes and high southern latitudes. Micropaleontology 30: 319-342

Fenner J (1985) Late Cretaceous to Oligocene planktic diatoms. In: Bolli HM, Saunders JB, Perch-Nielsen K (eds) Plankton Stratigraphy, pp 413-456

Fildani A, Hessler AM, Graham SA (2008) Trench-forearc interactions reflected in the sedimentary fill of the Talara basin, northwest Peru. . Basin Res. 20: 305–331

Fioroni C, Villa G, Persico D, Jovane L (2015) Middle Eocene-Lower Oligocene calcareous nannofossil biostratigraphy and paleoceanographic implications from Site 711 (equatorial Indian Ocean). Marine Micropaleontology 118

Fornaciari E, Agnini C, Catanzariti R, Rio D, Bolla EM, Valvasoni E (2010) Mid-Latitude calcareous nannofossil biostratigraphy and biochronology across the middle to late Eocene transition. Stratigraphy 7: 229-264

Fourtanier E, Macharé J (1988) Late Eocene to Pliocene marine diatoms from Peru. In: Round FE (ed) Proc. Ninth Int. Diatom Symp., Bristol. Bristolpress, pp 151-163

Gariboldi K, Bosio G, Malinverno E, Gioncada A, Di Celma C, Villa IM, Urbina M, Bianucci G (2017) Biostratigraphy, geochronology and sedimentation rates of the upper Miocene Pisco Formation at two important marine vertebrate fossil-bearing sites of southern Peru. Newsletters on Stratigraphy 50: 417-444

Gibbs SJ, Bralower TJ, Bown PR, Zachos JC, Bybell LM (2006) Shelf and open-ocean calcareous phytoplankton assemblages across the Paleocene–Eocene Thermal Maximum: implications for global productivity gradients. Geology 34: 233-236

Gioncada A, Collareta A, Gariboldi K, Lambert O, Di Celma C, Bonaccorsi E, Urbina-Schmitt M, Bianucci G (2016) Inside baleen: exceptional microstructure preservation in a late Miocene whale skeleton from Peru. Geology 44: 839-842

Gioncada A, Gariboldi K, Collareta A, Di Celma C, Bosio G, Malinverno A, Lambert O, Pike J, Urbina-Schmitt M, Bianucci G (2018) Looking for the key to preservation of fossil marine vertebrates in the Pisco Formation of Peru: new insights from a small dolphin skeleton. Andean Geology 45: 379-398

Gladenkov AY (2013) First Finds of Eocene Diatoms in the Marine Paleogene Reference Section in the Il'pinskii Peninsula, Northeastern Kamchatka. Stratigraphy and Geological Correlation 21: 96-106

Goldner A, Herold N, Huber M (2014) Antarctic glaciation caused ocean circulation changes at the Eocene–Oligocene transition. Nature 511: 7511-7514

Gombos AM (1976) Paleogene and Neogene diatoms from the Falkland Plateau and Malvinas outer basin: Leg 36, Deep Sea Drilling Project. In: Barker P, Dalziel IWD, Dinkelman MG, Elliott DH, Gombos AM,

Jr., Lonardi A, Plafker G, Tarney J, Thomson RW, Tjalsma RC, von der Borch CC, Wise SW, Jr. (eds) Initial Reports of the Deep Sea Drilling Project, pp 575-687

Gradstein F.M., Ogg J.G., Schmitz M., Ogg G. (2020). Geologic Time Scale 2020. Elsevier, 1390 pp.

Guerreiro C, Cachão M, Drago T (2005) Calcareous nannoplankton as a tracer of the marine influence on the NW coast of Portugal, over the last 14,000 years. J. Nannoplankton Res 27: 159–172

Hajós M (1976) Upper Eocene and lower Oligocene diatomaceae, Archaeomonadaceae, and Silicoflagellatae in the Southwestern Pacific sediments, Leg 29. In: Hollister CD, Craddock C, al. e (eds) Initial Reports of the Deep Sea Drilling Project, pp 817-883

Harwood DM, Bohaty S (2001) Early Oligocene Siliceous Microfossil Biostratigraphy of Cape Roberts Project Core CRP-3, Victoria Land Basin, Antarctica. Terra Antarctica 8: 315-338

Herbozo G, Kukowski N, Clift PD, Pecher I, Bolaños,R (2020) Cenozoic increase in subduction erosion during plate convergence variability along the convergent margin off Trujillo, Peru. Tectonophysics 790, article #228557.

Higley DK (2004) The Talara Basin Province of Northwestern Peru: Cretaceous-Tertiary Total Petroleum System. U.S. Geological Survey Bulletin 2206-A: 1-20

Ibaraki M (1993) Eocene to Early Miocene Planktonic Foraminifera from the South of Paracas, Central Peru. Reports of the Faculty of Science, Shizuoka University 27: 77-93

Kalb AL, Bralower TJ (2012) Nannoplankton origination events and environmental changes in the late Paleocene and early Eocene. Marine Micropaleontology 92-92: 1-15

Kemp ES, Pike J, Pearce RB, Lange CB (2000) The "Fall dump" - a new perspective on the role of a `shade flora in the annual cycle of diatom production and export flux. Deep-Sea Research II 47: 2129-2154

Koç N, Scherer RP (1996) Neogene Diatom Biostratigraphy of the Iceland Sea Site 9071 Proceedings of the Ocean Drilling Program. Scientific Results, pp 61-74

Lagabrielle Y, Goddéris Y, Donnedieu Y, Malavieille J, Suarez M (2009) The tectonic history of Drake Passage and its possible impacts on global climate. Earth and Planetary Science Letters 279: 197-211

Lambert O, Bianucci G, Salas-Sigismondi R, Di Celma C, Sterbaut E, Urbina M, de Muizon C (2019) An Amphibious Whale from the Middle Eocene of Peru Reveals Early South Pacific Dispersal of Quadrupedal Cetaceans. Current Biology 29: 1352-1359

Lambert O, Collareta A, Benites-Palomino AM, Di Celma C, de Muizon C, Urbina M, Bianucci G (2020a) A new small, mesorostrine inioid (Cetacea, Odontoceti, Delphinida) from four upper Miocene localities in the Pisco Basin, Peru. Papers in Paleontology

Lambert O, Collareta A, Landini W, Post K, Ramassamy B, Di Celma C, Urbina-Schmitt M, Bianucci G (2015) No deep diving: evidence of predation on epipelagic fish for a stem beaked whale from the Late Miocene of Peru. Proceedings of the National Academy of Sciences 282: article #20151530

Lambert O, de Muizon C, Malinverno E, Di Celma C, Urbina M, Bianucci G (2017a) A new odontocete (toothed cetacean) from the Early Miocene of Peru expands the morphological disparity of extinct heterodont dolphins. Journal of Systematic Palaeontology

Lambert O, De Muizon C, Urbina M, Bianucci G (2020b) A new longirostrine sperm whale (Cetacea, Physeteroidea) from the lower Miocene of the Pisco Basin (southern coast of Peru). Journal of Systematic Palaeontology 18: 1707-1742

Lambert O, Martinez-Caceres M, Bianucci G, Di Celma C, Salas-Sigismondi R, Sterbaut E, Urbina M, de Muizon C (2017b) Earliest Mysticete from the Late Eocene of Peru Sheds New Light on the Origin of Baleen Whales. Current Biology 22: 1-7

Landini W, Altamirano-Sierra A, Collareta A, Di Celma C, Urbina-Schmitt M, Bianucci G (2017a) The late Miocene elasmobranch assemblage from Cerro Colorado (Pisco Formation, Peru). Journal of South American Earth Sciences 73

Landini W, Collareta A, Di Celma C, Malinverno A, Urbina-Schmitt M, Bianucci G (2019) The early Miocene elasmobranch assemblage from Zamaca (Chilcatay Formation, Peru). Journal of South American Earth Sciences 91: 352-371

Landini W, Collareta A, Pesci F, Di Celma C, Urbina-Schmitt M, Bianucci G (2017b) A secondary nursery area for the copper shark Carcharhinus brachyurus from the late Miocene of Peru. Journal of South American Earth Sciences 78: 164-174

Léon W, Aleman A, Torres V, Rosell W, De La Cruz O (2008) Estratigrafía, sedimentología y evolución tectónica de la Cuenca Pisco Oriental. Boletin INGEMMET (serie D) 27: 1-144

Lisson CI (1925) Algunos fosiles de Paracas. Bol. Soc. Geol. Peru 1: 23–30

Macharé J, deVries TJ, Barron J, Fourtanier E (1988) Oligo-Miocene transgression along the Pacific margin of South America: new paleontological and geophisical evidence from the Pisco Basin. Géodynamique 3: 25-37

Macharé J, Fourtanier E (1988) Datation des formations tertiaires du bassin de Pisco (Pérou) à partir d'associations de diatoméès. C.R. Acad. Sci. Paris 305

Martínez-Cáceres M, de Muizon C (2011) A new basilosaurid (Cetacea, Pelagiceti) from the Late Eocene to Early Oligocene Otuma Formation of Peru. C.R. Palevol 10: 517-526

Martínez-Cáceres M, Lambert O, de Muizon C (2017) The anatomy and phylogenetic affinities of Cynthiacetus peruvianus, a large Dorudon-like basilosaurid (Cetacea, Mammalia) from the late Eocene of Peru. Geodiversitas 39: 7-163

Martini E (1971) Standard Tertiary and Quaternary calcareous nannoplankton zonation. In: Farinacci A (ed) Proceedings 2nd International Conference Planktonic Microfossils Roma. Ed. Tecnosci, Rome, pp 739-785

Martini E (1990a) Tertiary and Quaternary calcareous nannoplankton biostratigraphy off Peru (ODP Leg 112). In: Suess E, von Huene R, al. e (eds) Proceedings of the Ocean Drilling Program, Scientific Results, pp 217-238

Martini E (1990b) Tertiary and Quaternary silicoflagellates, actiniscidians, and ebridians from the eastern Pacific off Peru (Leg 112). In: Suess E, Von Huene R, al. e (eds) Proceedings of Ocean Drilling Program, Scientific Results, pp 157-173

Marty R, Dunbar R, Martin JB, Baker P (1988) Late Eocene diatomite from the Peruvian coastal desert, coastal upwelling in the eastern Pacific, and Pacific circulation before the terminal Eocene event. Geology 16: 818-822

Marty RC (1989) Stratigraphy and chemical sedimentology of Cenozoic biogenic sediments from the Pisco and Sechura Basins, Peru. PhD Thesis, Rice University

Marx F, Collareta A, Gioncada A, Post K, Lambert O, Bonaccorsi E, Bianucci G (2017) How whales used to filter: exceptionally preserved baleen in a Miocene cetotheriid. Journal of Anatomy 231: 212-220

Marx F, Uhen MD (2010) Climate, critters, and cetaceans: Cenozoic drivers of the evolution of modern whales. Science 327: 993-996

McCartney K, Witkowski J, Nowakowski R, Szaruga A, Wróbel R, Zglobicka I (2020) Evolution of the silicoflagellate naviculopsid skeletal morphology in the Cenozoic. Marine Micropaleontology 156: 101820

Monechi S, Buccianti A, Gardin S (2000) Biotic signals from nannoflora across the iridium anomaly in the upper Eocene of the Massignano section: evidence from statistical analysis. Marine Micropaleontology 39: 219-237

Moore TC, Wade B, Westerhold T, Erhardt AM, Coxall HK, Baldauf J, Wagner M (2014) Equatorial Pacific productivity changes near the Eocene-Oligocene boundary. Paleoceanography 29: 825-844

Morales-Reyna MC, Chacaltana-Budiel C, Valdivia-Vera W (2010) Lepidocyclina (Lepidocyclina) peruviana (CUSHMAN) en la Cuenca Pisco: geocronologia y paleoambiente. Sociedad Geológica del Perú, Special Publication, Lima 9: 237-240

Morales-Reyna MC, Tejada-Medina L, Chacaltana-Budiel C (2013) Significado de la presencia del foraminifero Amphistegina sp. del Paleógeno en la cuenca Pisco. I Simposio Internacional de Paleontologia del Perú, Libro de Resúmenes.- INGEMMET, Lima, : 29-31

Musaka S, Henry DJ (1990) The San Nicolás batholith of coastal Peru: Early Palaeozoic continental arc or continental rift magmatism? Journal of the Geological Society, London 147: 27-39

Narvàez-Rodriguez Y, Pardo-Arguedas A (2009) Nannofossil biostratigraphy of Eocene strata in the Talara Basin, Peru. In: Demchuk TD, Gary AC (eds) Geologic Problem Solving with Microfossils: a volume in Honor of Garry D. Jones. SEPM Special Publication, pp 287-291

Narvàez-Rodriguez Y, Setembrino P (2001) Calcareous nannofossil biostratigraphy of the Talara group (Middle-Late Eocene) in the Negritos and Carpitas fields, Talara Basin, Peru. Journal of Nannoplankton Research 23: 9-13

Nilsen EB, Anderson LD, Delanei ML (2003) Paleoproductivity, nutrient burial, climate change and the carbon cycle in the western equatorial Atlantic across the Eocene/Oligocene boundary. Paleoceanography 18: 1057

Norris RD, Kirtland Turner S, Hull PM, Ridgwell A (2013) Marine ecosystem responses to Cenozoic global change. Science 341: 492-498

Okada H, Bukry D (1980) Supplementary modification and introduction of code numbers to the low-latitude coccolith biostratigraphic zonation (Bukry 1973, 1975). Marine Micropaleontology 5: 321-325

Olsson AA (1928) Contributions to the Tertiary paleontology of northern Peru: Part I, Eocene Mollusca and Brachiopoda. Bulletins of American Paleontology 14: 155 pp.

Olsson AA (1930) Contributions to the Tertiary Paleontology of Northern Peru; Part 3. Eocene Mollusca. Bulletins of American Paleontology 17: 73 pp

Onodera J, Takahashi K (2009) Middle Eocene ebridians from the central Arctic Basin. Micropaleontology 55: 187-208

Oreshkina TV, Aleksandrova GN (2007) Terminal Paleocene of the Volga Middle Reaches: Biostratigraphy and Paleosettings. Stratigraphy and Geological Correlation 15: 206-230

Oreshkina TV, Radionova EP (2014) Diatom record of the Paleocene-Eocene Thermal Maximum in marine paleobasins of Central Russia, Transuralia and adjacent regions. Nova Hedwigia, Beiheft 143: 307-336

Pälike H, Lyle M, Nishi H, Raffi I, Ridgwell A, Kusali G, Klaus A, Acton G, Anderson L, Backman J, Baldauf J, Beltran C, Bohaty S, Bown PR, Busch, Channel JET, Chun CO, Delaney M, Dewangan P, Dunkley Jones T, Edgar K, Evans H, Fitch P, Foster GL, Gussone N, Hasegawa H, Hathorne EC, Hayashi H, Herrle JO, Holbourn A, Hovan S, Hyeong K, Iijima K, Ito K, Kamimuri S, Kimoto K, Kuroda J, Leon-Rodriguez L, Malinverno A, Moore TC, Murphy BH, Murphy DP, Nakamura H, Ogane K, Ohneiser C, Richter C, Robinson R, Rohling E, Romero O, Sawada k, Scher H, Schneider L, Sluis A, Takata H, Tian J, Tsujimoto A, Wade B, Westerhold T, Wilkens R, Williams T, Wilson PA, Yamamoto Y, Yamamoto S, Yamazaki T, Zeebe RE (2012) A Cenozoic record of the equatorial Pacific carbonate compensation depth. Nature 488: 609-615

Perch-Nielsen K (1985a) Cenozoic calcareous nannofossils. In: Bolli HM, Saunders JB, Perch-Nielsen K (eds) Plankton Stratigraphy. Cambridge Earth Science Series, pp 427-554

Perch-Nielsen K (1985b) Silicoflagellates. In: Bolli HM, Saunders JB, Perch-Nielsen K (eds) Plankton Stratigraphy. Cambridge Earth Science Series, pp 811-846

Persico D, Villa G (2004) Eocene–Oligocene calcareous nannofossils from Maud Rise and Kerguelen Plateau /Antarctica): paleoecological and paleoceanographic implications. Marine Micropaleontology 52: 153-179

Petersen G (1954) Informe preliminar sobre la geologia de la faja costerna del departamento de Ica. Bol. Tec. Empresa Petrol. Fisc. 1: 33-61

Prudhomme A, Baby P, Robert A, Brichau S, Cuipa E, Eude A, Calderon Y, O'Sullivan P (2019) Western thrusting and uplift in northern Central Andes (western Peruvian margin) Andean Tectonics, pp 299-331

Ramos VA (2008). The basement of the Central Andes: The Arequipa and related terranes. Annual Review of Earth and Planetary Sciences, 36, 289-324

Rea DK, Lyle MW (2005) Paleogene calcite compensation depth in the eastern subtropical Pacific: answers and questions. Paleoceanography: 20 PA1012

Rivera R (1957) Moluscos fosiles de la formacion Paracas. dpto. de Ica. Bol. Soc. Geol. Peru 32: 165–219

Scherer RP, Gladenkov AY, Barron JA (2007) Methods and applications of Cenozoic marine diatom biostratigraphy. In: Starratt S (ed) Pond Scum to Carbon Sink: Geological and Environmental Applications of the Diatoms, Paleontological Society Short Course, October 27, 2007. Paleontological Society Papers. The Paleontological Society, pp 61-83

Schrader H, Castaneda JC (1990) The Ballena and Delfin wells off central Peru: revised ages. In: Suess E, Von Huene R, al. e (eds) Proceedings of the Ocean Drilling Program, Scientific Results, pp 209-215

Sims PA, Fryxell G, Baldauf JG (1989) Critical examination of the diatom genus Azpeitia; species useful as biostratigraphic markers for the Oligocene and Miocene epochs. Micropaleontology 35: 293-307

Skilbeck CG, Fink D (2006) Radiocarbon dating and sedimentation rates for Holocene–upper Pleistocene sediments, eastern equatorial Pacific and Peru continental margin. In: Jørgensen BB, D'Hondt SL, Miller DJ (eds) Proc. ODP, Sci. Results, pp 1-15

Solís Mundaca FA (2018) Bioestratigrafía y implicancias paleoceanográficas de las diatomeas de la sección Cerro Caucato, Formación Pisco, Ica, Perù, Lima, Peru

Strelnikova NI, Fourtanier E, Kociolek JP, Barron JA (2001) Ultrastructure studies of *Coscinodiscus* and *Cestodiscus* species from the Eocene and Oligocene. In Lange-Bertalot Fest Schrift. Studies on Diatoms. Dedicated to prof. Dr. hc Horst Lange-Bertalot On the occasion of his 65th Birthday, pp 63-96.

Suess E, Von Huene R (1988) Proceedings of the Ocean Drilling Program, Initial Reports112: 5-23

Suto I, Kawamura K, Hagimoto S, Teraishi A, Tanaka Y (2012) Changes in upwelling mechanisms drove the evolution of marine organisms. Palaeogeography, Palaeoclimatology, Palaeoecology 339-341: 39-51.

Thornburg T, Kulm LD (1981) Sedimentary basins of the Peru continental margin: Structure, stratigraphy and Cenozoic tectonics from 6° to 16° S latitude. In: Kulm LD, and others (eds) Nazca Plate: Crustal Formation and Andean Convergence. Geological Society of America Memoir, pp 393-422

Toffanin F, Agnini C, Rio D, Acton G, Westerhold T (2013) Middle Eocene to early Oligocene calcareous nannofossil biostratigraphy at IODP Site U1333 (equatorial Pacific). Micropaleontology 59: 69-82

Tsoy IB (2011) Silicoflagellates of the Middle–Early Late Eocene of the Kronotskii Bay (Eastern Kamchatka). Stratigraphy and Geological Correlation 19: 87-101

Tsuchi R, Koizumi I, Ibaraki M, Aldana A, Villavicencio E (1992) Fundamental data on Cenozoic biostratigraphy of the Pacific coast of Peru - Supplement 2. Reports of andean studies, Shizuoka University, special volume 4: 33-40

Tsuchi R, Shuto T, Takayama T, Fujiyoshi A, Koizumi I, Ibaraki M, Rangel C, Aldana A (1988) Fundamental data of Cenozoic biostratigraphy of the Pacific coast of Peru. Reports of andean studies, Shizuoka University, special volume 2: 45-70

Uhen MD, Pyenson ND, deVries TJ, Urbina M, Renne PR (2011) New middle Eocene whales from the Pisco Basin of Peru. Journal of Paleontology 85: 955-969

Villa G, Fioroni C, Pea L, Bohaty S, Persico D (2008) Middle Eocene–late Oligocene climate variability: Calcareous nannofossil response at Kerguelen Plateau, Site 748. Marine Micropaleontology 69: 173-192

Villa G, Fioroni C, Persico D, Roberts AP, Florindo F (2014) Middle Eocene to Late Oligocene Antarctic glaciation/deglaciation and Southern Ocean productivity. Paleoceanography PA002518: 223-227

Von Huene, R. and Lallemand, S., 1990. Tectonic erosion along the Japan and Peru convergent margins. Geol. Soc. Am. Bull, 102: 704-720

Von Huene R, Suess E, Scientists aLS (1988) Ocean Drilling Program Leg 112, Peru continental margin: Part 1, tectonic history. Geology 16: 934-938

Wei W, Villa G, Wise SW, Jr. (1992) Paleoceanographic implications of Eocene-Oligocene calcareous nannofossils from sites 711 and 748 in the Indian Ocean. In: Wise SW, Jr., Schlich R, al. e (eds) Proc. ODP, Sci. res, pp 979-999

Wei W, Wise SW, Jr. (1990) Middle Eocene-Oligocene calcareous nannoplankton biogeographic gradient of the South Atlantic Ocean. Palaeogeography, Palaeoclimatology, Palaeoecology 79: 29-61

Westerhold T, Röhl U (2013) Orbital pacing of Eocene climate during the Middle Eocene Climate Optimum and the chron C19r event: Missing link found in the tropical western Atlantic. Geochem. Geophys. Geosyst. 14: 4811-4825

Westerhold T., Marwan N., Drury A.J., Liebrand D., Agnini C., Anagnostou E., Barnet J.S.K., Bohaty S.M., De Vleeschouwer D., Florindo F., Frederichs T., Hodell D.A., Holbourn A.E., Kroon D., Lauretano V., Littler K., Lourens L.J., Lyle M., Pälike H., Röhl U., Tian J., Wilkens R.H., Wilson P.A., Zachos J.C. (2020) An astronomically dated record of Earth's climate and its predictability over the last 66 million years. Science 369: 1383–1387

Witkowski J, Bohaty SM, Edgar K, Harwood DM (2014) Rapid Fluctuations in Mid-Latitude Siliceous Plankton Production during the Middle Eocene Climatic Optimum (ODP Site 1051, Western North Atlantic). Micropaleontology 106: 110-129

Witkowski J, Harwood DM, Wade BS, Brylka K (2020) Rethinking the chronology of early Paleogene sediments in the western North Atlantic using diatom biostratigraphy. Marine Geology 424: 106168

Young JR, Bown PR, Lees JA (2020) Nannotax3 website. International Nannoplankton Association. Accessed 21 Nov. 2020. URL: http://www.mikrotax.org/Nannotax3

Zachos JC, Dickens GR, Zeebe RE (2008) An early Cenozoic perspective on greenhouse warming and carbon-cycle dynamics. Nature 541: 279-283

Zachos JC, Pagani M, Sloan L, E. T, Billups K (2001) Trends, Rhytms and aberrations in global climate 65 Ma to present. Science 292: 686-693

Ziveri P, Baumann K-H, Bockel B, Bollmann J, Young JR (2004) Biogeography of selected Holocene coccoliths in the Atlantic Ocean. In: Thierstein HR, Young JR (eds) Coccolithophores — From Molecular Processes to Global Impact. Springer-Verlag, Berlin Heidelberg, pp 403–428